Hydrogeological control on carbon dioxide input into the atmosphere of the Chauvet-Pont d'Arc cave

François Bourges, Dominique Genty, Frédéric Perrier, Bruno Lartiges, Édouard Régnier, Alexandre François, Johann Leplat, Stéphanie Touron, Faisl Bousta, Marc Massault, et al.

Contents lists available at ScienceDirect

Science of the Total Environment

journal homepage: http://ees.elsevier.com

Hydrogeological control on carbon dioxide input into the atmosphere of the Chauvet-Pont d'Arc cave

François Bourges [a], Dominique Genty [b], Frédéric Perrier [c,*], Bruno Lartiges [d], Édouard Régnier [b], Alexandre François [e], Johann Leplat [e], Stéphanie Touron [e], Faisl Bousta [e], Marc Massault [f], Marc Delmotte [b], Jean-Pascal Dumoulin [g], Frédéric Girault [c], Michel Ramonet [b], Charles Chauveau [h], Paulo Rodrigues [h]

[a] Géologie Environnement Conseil, 30 rue de la République, F-09200 Saint-Girons, France
[b] Laboratoire des Sciences du Climat et de l'Environnement, CNRS, F-91691 Gif-sur-Yvette, France
[c] Institut de Physique du Globe de Paris, Université de Paris, 1 rue Jussieu, F-75005 Paris, France
[d] Université de Toulouse III Paul Sabatier, Géosciences Environnement-Toulouse, 14 av. Edouard Belin, F-31400 Toulouse, France
[e] Laboratoire de Recherches des Monuments Historiques (CRC, USR3224), Museum national d'Histoire naturelle, Sorbonne Universités, Ministère de la Culture, CRNS, 29 rue de Paris, F-77420 Champs-sur-Marne, France
[f] Laboratoire Interactions et Dynamique des Environnements de Surface, Université Paris Sud, F-91405 Orsay, France
[g] Laboratoire de Mesure du Carbone 14 (LMC14), LSCE/IPSL, CEA-CNRS-UVSQ, Université Paris-Saclay, F-91191 Gif-sur-Yvette, France
[h] Service de la Conservation de la Grotte Chauvet, Ministère de la Culture, F-07150 Vallon-Pont-d'Arc, France

ARTICLE INFO

Article history:
Received 27 March 2019
Received in revised form 16 January 2020
Accepted 20 January 2020
Available online xxx
Editor: Jay Gan

Keywords
Underground
Carbon dioxide
Vadose zone
Natural ventilation
Painted cave
Preservation

ABSTRACT

Carbon dioxide (CO_2) concentration (CDC) is an essential parameter of underground atmospheres for safety and cave heritage preservation. In the Chauvet cave (South France), a world heritage site hosting unique paintings dated 36,000 years BP, a high-sensitivity monitoring, ongoing since 1997, revealed: 1) two compartments with a spatially uniform CDC, a large volume (A) (40,000 to 80,000 m^3) with a mean value of 2.20 ± 0.01% vol. in 2016, and a smaller remote room (B) (2000 m^3), with a higher mean value of 3.42 ± 0.01%; 2) large CDC annual variations with peak-to-peak amplitude of 2% and 1.6% in A and B, respectively; 3) long-term changes, with an increase of CDC and of its annual amplitude since 1997, then faster since 2013, reaching a maximum of 4.4% in B in 2017, decreasing afterwards. While a large effect of seasonal ventilation is ruled out, monitoring of seepage at two dripping points indicated that the main control of CDC seasonal reduction was transient infiltration. During periods of water deficit, calculated from surface temperature and rainfall, CDC systematically increased. The carbon isotopic composition of CO_2, correlated with water excess, is consistent with a time-varying component of CO_2 seeping from above. The CO_2 flux, which is the primary driver of CDC in A and B, inferred using box modelling, was found to confirm the relationship between water excess and reduced CO_2 flux into A, compatible with a more constant flux into B. A buoyancy-driven horizontal CO_2 flow model in the vadose zone, hindered by water infiltration, is proposed. Similarly, pluri-annual and long-term CDC changes can likely be attributed to variations of water excess, but also to increasing vegetation density above the cave. As CDC controls the carbonate geochemistry, an increased variability of CDC raises concern for the preservation of the Chauvet cave paintings.

1. Introduction

The preservation of the exceptionally precious heritage of painted caves in the context of a rapidly evolving environment (Pla, 2016; Dominguez-Villar et al., 2014; Beltrami et al., 2005; Perrier et al., 2005a; Badino, 2004) represents a challenging issue for the scientific community (Bourges et al., 2014a, 2014b; Baker and Genty, 1998). While the prehistoric paintings have reached present times owing to particularly stable underground conditions (Mangin et al., 1999; Quindos et al., 1987), caves are affected by global and local changes (Pla, 2016; Baker and Genty, 1998), by visitors (Saiz-Jimenez et al., 2011; Fernandez-Cortes et al., 2011; Hoyos et al., 1998; Villar et al., 1984, 1986), and by mistaken remediation strategies, difficult to reverse, as in the case of the Lascaux cave in France (Martin-Sanchez et al., 2012, 2014). One essential parameter controlling the chemical conditions at the wall surface, and in particular dissolution and precipitation of carbonates and speleothem growth, is the CO_2 concentration (CDC) in the cave atmosphere (Houillon et al., 2017; Spötl et al., 2005; Genty and Deflandre, 1998). Conversely, this parameter provides information about the evolution of the underground microclimate and of its thermodynamical conditions, as well as of its surroundings (Bourges et al., 2012; Fernandez-

* Corresponding author.
E-mail address: perrier@ipgp.fr (F. Perrier)

https://doi.org/10.1016/j.scitotenv.2020.136844
0048-9697/

Cortes et al., 2011). Thus, one key issue for the understanding of the preservation and degradation processes, and for the monitoring of the effect of remediation, is the characterization of CO_2 sources and transport modes into and out of the underground cavities (Houillon et al., 2017).

Various atmospheric and underground CO_2 sources can be distinguished. In volcanic regions, the major source of CO_2 is the degassing of mantle rocks, characterized by an isotopic carbon ratio $\delta^{13}C$ of $-2.3 \pm 0.9‰$ (Chiodini et al., 2008). Crustal CO_2 from metamorphic decarbonation (Groppo et al., 2017), characterized by $\delta^{13}C$ values in the range -0.9 to $-0.7‰$, was shown to accumulate in a tunnel near active faults in the Nepal Himalayas (Girault et al., 2014, 2018). While important in principle, given the large fluxes from the ground, often in excess of 10^5 g/m^2/day, mantle and crustal CO_2 sources are not main contributors in the case of European painted caves. Instead, the major relevant production source is the biogenic production from the soil and the epikarst (Mattey et al., 2016; Faimon et al., 2012; Bourges et al., 2001; Atkinson, 1977), or in the underground part of the critical zone (CZ), defined as the domain included from the base of the aquifer to the top of the canopy (Lin, 2010).

Two main zones of CO_2 production can be distinguished (Peyraube et al., 2013, 2018; Mattey et al., 2016): 1) soil CO_2 (SC), which includes the emission of CO_2 by microorganisms and root respiration, and 2) ground CO_2 (GC), which includes CO_2 released by the decay of organic matter in the vadose zone. The combined analysis of $\delta^{13}C$ ratio and ^{14}C activity of carbon dissolved in seepage water and in speleothems further indicates that the CO_2 above the cave can be modelled by several compartments with different residence times, mainly controlled by soil organic matter (SOM) degradation rates, which, in this example, integrates SC and GC (Genty and Massault, 1997, 1999). SC is characterized, under typical C3 type (Calvin–Benson photosynthetic pathway) vegetation growing above the cave, by $\delta^{13}C$ values of the order of $-26‰$ or smaller (Mattey et al., 2016; Genty et al., 1998; Dörr and Münnich, 1986; Fleyfel, 1979) and CDC can reach values from 1 to about 3% (% refers to % vol. throughout the paper). The ^{14}C activity of the SC and GC produced by the biological activity is similar to the ^{14}C activity of the outside atmosphere, unless the decaying organic matter is significantly aged (Genty and Massault, 1999). GC, when it can be isolated from SC, for example in boreholes where air from the surrounding epikarst porous space can accumulate (Houillon et al., 2017; Mattey et al., 2016; Benavente et al., 2010; Wood, 1985; Wood and Petraitis, 1984), is slightly heavier isotopically, from $-24‰$ to $-18‰$ (Mattey et al., 2016), and CDC can be higher than 5% (Houillon et al., 2017; Ek and Gewelt, 1985). The reason why SC is heavier is that the addition of higher level of CO_2 from the decay of organic matter in an enclosed space (epikarst porosity) requires the dissolution of extra bedrock to attain equilibrium (Mattey et al., 2016). The outside atmosphere provides another important source of CO_2, with CDC around 390 ppm, constantly increasing (Dlugokencky et al., 2018), characterized by a slowly decreasing isotopic composition with $\delta^{13}C = -8.3‰$ in 2010 (Graven et al., 2017). In the atmosphere, the ^{14}C signature is still in the end of the post-bomb decreasing trend (Graven et al., 2017), close to 102 pMC (percent Modern Carbon). Ultimately, cave air CDC results from mixing and interactions of these various sources and their corresponding fluxes at the boundaries of air volumes of the cavity.

The main input of outside air into the underground atmosphere is natural ventilation, essentially driven by the buoyancy difference between outside varying air and cave interior quasi-stable air (Fernandez-Cortes et al., 2009; Linden et al., 1990). This buoyancy difference is mainly controlled by the temperature difference of air masses, but the effects of moisture and CO_2 content can also be significant (De Freitas and Littlejohn, 1987; De Freitas et al., 1982). In addition, variations of atmospheric pressure (barometric pumping) coherently displace air masses and produce cave breathing (Perrier and Le Mouël, 2016; Wigley, 1967). A decrease in atmospheric pressure leads to the extraction of porous space air and of the cavity air to the outside, while an increase in atmospheric pressure leads to outside air being pushed into underground spaces. Close to the entrances or in the case of important porous dry volumes, large effective air volumes downstream can lead to spectacular motions referred to as "cave wind" (Conn, 1966). This pumping process is frequency-dependent and efficiently mixes cave air and outside air; it supplements natural ventilation, and sometimes even dominates (Perrier and Richon, 2010).

Additional processes for CO_2 transport occur within the underground cavities. One important process, particularly in the epikarst, is the degassing of dripping water (Houillon et al., 2017; Balakowicz and Jusserand, 1986), which can be significant in CO_2-poor atmospheres, especially during episodes of enhanced transient infiltration and subsequent seepage. Reservoirs of SC and GC contribute to cave air both by diffusion processes, which dominates in the poorly-connected porosity of the surrounding micro-fractured rock, and by buoyancy-driven processes (Mattey et al., 2016; Badino, 2009), dominant through well-connected porosity networks. Indeed, CO_2-richer, drier or colder air tends to flow downwards while CO_2-poorer, more humid or warmer air raises through connected networks, for example through a discrete number of well-connected fracture networks, while most of the encasing porosity remains as a passive static reservoir. In the case of karstic domains, networks can include, besides fractures, large conduits, sometimes occupied by water (Zhang et al., 2017). In addition, purely advective processes, associated with pressure gradients can enhance air motion and CO_2 release into the underground even in the absence of buoyancy-driven flows (Lang et al., 2017). Finally, mixed processes can occur in the vadose zone, for example washout of pore air by small water pockets (piston effects) through destabilized capillaries (Genty and Deflandre, 1998). In the epikarst, fast rain infiltration also results in sudden pressure increases of the pore air, further facilitating air displacement. The cave air CDC and the associated isotopic signatures result from the relative contributions of these various transport processes. Internal mixing (Houillon et al., 2017; Perrier and Richon, 2010), besides ventilation processes, also plays an important role in the spatial and temporal variations of the cavity CDC. Disentangling the various sources of CO_2, their interactions, and the various mixing and transport mechanisms resulting into the observed CDC in a cave remains a heuristic and challenging task (Cuezva et al., 2011). In some cases, CDC can reach a few %: 2 to 2.6% in the Pech Merle cave (Bourges et al., 2014a), 2 to 3% in the Lascaux cave (Houillon et al., 2017), up to 4% in the Aven d'Orgnac (Bourges et al., 2001, 2006; Mangin et al., 1999), or as large as 6% in the Grandes Combes cave (Batiot-Guilhe et al., 2007). Such high CDC values also lead to substantial health issues (Roberson-Nay et al., 2017; Smith, 1993; Brodovsky et al., 1960).

In this study, we establish basic features of CDC in the atmosphere of the Chauvet cave, South-East France, a world heritage site containing a unique set of elaborated prehistoric paintings dated 36,000 BP, and one of the oldest human art sites in the world (Clottes et al., 1995). We summarize the behaviour of CDC since the monitoring of the Chauvet cave started in 1997, and we focus on the period from 2014 to 2019 when more comprehensive records are available. We exhibit the dominating importance of water infiltration on temporal variations of CDC. Finally, we discuss the relevance of these findings for preservation.

2. The Chauvet painted cave

2.1. Geological and geographical contexts

The Chauvet-Pont d'Arc cave (44°13.8′N, 4°15′E) is located in South-East France on the left bank of the Ardèche river, a tributary

of the Rhône river, in an Upper Barremian (Lower Cretaceous, Urgonian type) limestone cliff above an abandoned meander (Bourges et al., 2014a, 2014b; Clottes et al., 1995). The entrance (Fig. 1) is a narrow conduit above the slope collapse at an altitude of 200 m NGF. This conduit gives access from above to large chambers (Brunel, Bauges, and Hillaire Rooms) with a floor at elevation 186 to 188 m, and, through a smaller corridor (Megaceros Corridor) to a last and smaller room (Remote Room, hereinafter RR) with a lower floor at an altitude of about 179 m. The volume of the first set of chambers (Brunel, Bauges, and Hillaire Rooms) is estimated to amount about 60,000 ± 20,000 m^3, whereas the volume of the more isolated RR amounts to about 2000 ± 500 m^3.

The thickness of the limestone formation above the cave is about 50 m near the entrance and reaches 70 m in the deeper parts of the cavity, with a discontinuous covering layer of soil of varying thickness from a few decimeters to more than one meter at some rare places. Nowadays, the vegetation cover is dominated by bushes and deciduous or evergreen trees (*Quercus ilex* L.). However, the vegetation density has increased regularly at least for the last 70 years (Supp. Mat. Fig. 1). In 1980, the area was included in a nature reserve involving a free evolution of the plant communities.

2.2. Archaelogical content and its preservation

All rooms are decorated with sophisticated paintings of animals whose discovery, in 1994, caused a revolution in Paleolithic science (Clottes et al., 1995, 2001). The high level of refinement of the paintings showing perspective and movement in a large and elaborated scenic compositions is unique in prehistoric art; their age is now seriously well constrained by numerous radiocarbon dates (Quiles et al., 2016; Valladas et al., 2013) to the early period of Aurignacian corresponding to 33–36,000 BP, making them among the oldest prehistoric paintings in the world, and certainly the most exceptional. In addition to the paintings, various remains were found in the cave, including cave bear bones, charcoal, or flint tools. Some remains are covered by speleothems that have been accurately dated by uranium-thorium methods (Genty et al., 2004), confirming that some charcoals are older than 30,000 BP, and consequently establishing the age of the associated paintings. Despite their great age, the paintings in the Chauvet cave appear very fresh, human digits drawings on the wall are still intact, showing a remarkable preservation likely due to the closing of the cave caused by the collapse of the cliff above the entrance, dated 29–21,000 BP (Quiles et al., 2016; Sadier et al., 2012).

To avoid damage after the discovery in 1994, the cave was kept as much as possible in its original conditions: 1) the front screen that buffered the exchanges with the outside has been carefully preserved; 2) the small entrance of the discovery was enlarged to a minimum size allowing safe visits; 3) while maintaining as much as possible the natural air exchanges, a security door was installed at the front of the original rock shelter leading to the discovery pathway, now closed by a climatic door (Fig. 1a); 4) inside the cave, artificial pathways were constructed above the floor and severe access restrictions were implemented. In addition, a monitoring program of the cave microclimate was immediately initiated to provide information on possible changes in the cave conditions (Bourges et al., 2006, 2014a, 2014b).

2.3. Reference caves and meteorological observations

Several other caves in similar contexts have also been monitored after 1997, thus providing valuable references (Fig. 1). The closest cave reference is Aven d'Orgnac (44°19.11′N, 4°24.73′E), located 7 km to the South-East of the Chauvet cave (Bourges et al., 2001, 2006; Mangin et al., 1999), south of the right bank of the Ardèche river. It is a huge karstic volume in Aptian limestone of at least 240,000 m^3, reaching altitudes as low as 120 m, with a vertical access pit of 15 m height, opening at the surface of the limestone plateau, at an altitude

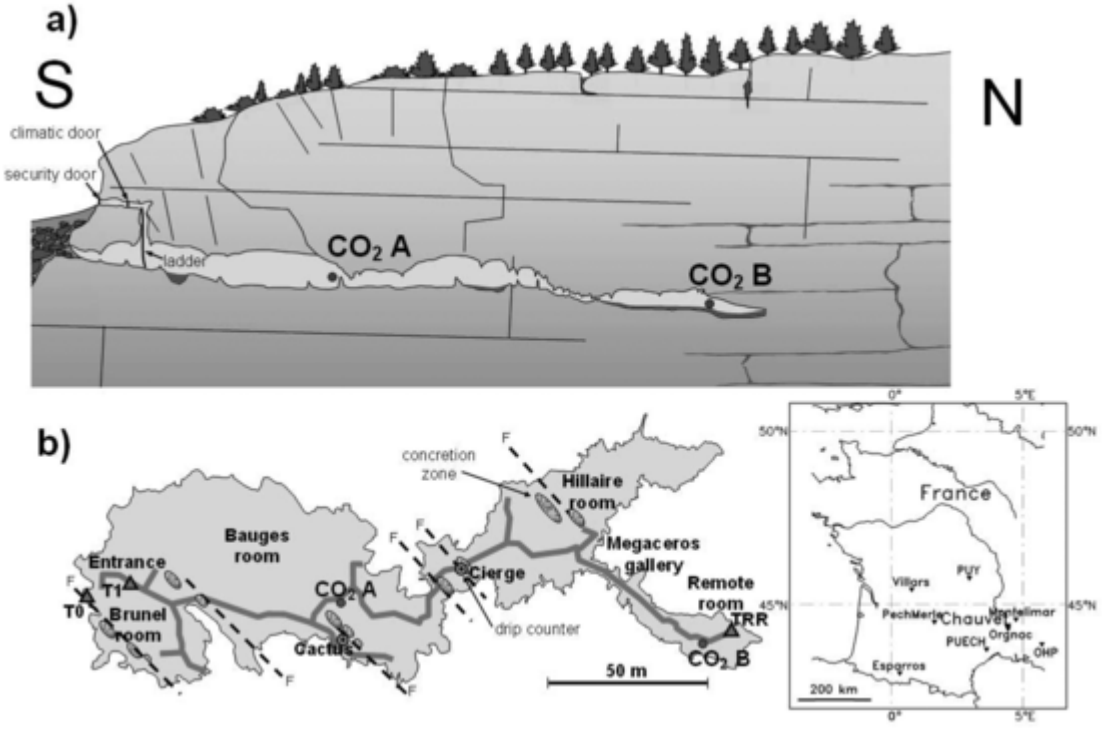

Fig. 1. a) Schematic simplified cross-section of the Chauvet cave. b) Position of the instruments in a simplified map of the cave (survey by Perazio Engineering, redrawn after Clottes et al., 2001). The letter F (b) indicates the presence of large scale fractures in the otherwise homogeneous limestone formation. The horizontal scale of the cross section (a) is the same as the map (b), but the vertical scale is exaggerated by 50%. The location of the Chauvet cave, the three reference caves (Esparros, Pech Merle, Aven d'Orgnac), as well as other sites and climatic observatories mentioned in this paper are shown in the inset.

of 300 m. Water level has been monitored in a 100 m deep borehole (44°17.517′N, 4°26.05′E), at an altitude of 170 m, 3 km from the Aven d'Orgnac. The Pech Merle painted cave (44°30.45′N, 1°48.67′E) is located on the Western edge of Massif Central in Oxfordian (Upper Jurassic) limestone and is characterized by an artificial entrance at 284 m, equipped with a double door, and a natural narrow opening at 302 m. The Gouffre d'Esparros cave (43°1.8′N, 0°19.8′E) is located in dolomitic limestone in the French Pyrenean foreland (Bourges et al., 2006). The Aven d'Orgnac, Pech Merle and Esparros caves are opened to visitors, with more than several hundreds visitors per day in the summer season. In addition to the data obtained at these reference caves, we also refer below to the Villars cave (Fig. 1), located in Jurassic limestone (Jean-Baptiste et al., 2019; Genty, 2008). We also used additional data from surface meteorological and climate observatories PUY, PUECH, Montélimar, and OHP (Fig. 1), and further details will be given when appropriate.

3. Instruments and methods

All sites are monitored with the same instruments and the same methodology. The data acquisitions with a sampling interval of 15 min are synchronized.

3.1. Monitoring of Chauvet cave climate

Several parameters have been continuously monitored since 1997, although several interruptions, due to storms or instrumental dysfunctions, have occurred between 2011 and 2013. Most of our attention, in the present study, is therefore focused on the period from 2014 to 2019.

The monitored parameters (Fig. 1b) include temperature at several locations, among which we focused, in this paper, on T1 (atmosphere and wall temperatures in Brunel Room) and TRR (atmosphere temperature in the RR). CDC was measured at two locations A (Bauges Room) and B (RR), whereas atmospheric pressure was monitored between the Bauges and Hillaire Rooms. CDC was measured 60 cm above the floor level, at an altitude of 186.83 m for A and 180.98 m for B. In addition, since 2013, temperature was monitored on the internal side of the collapse debris cone near the entrance (T0, see Fig. 1b). Radon-222 concentration was monitored near T0 and T1 using Barasol™ sensors from Algade (France), with a sampling interval of 15 min, from November 2014 to April 2015.

To measure temperature, we used Pt100 sensors recorded with a AOIP™, France, SA32 logger until 2013, then with a Campbell™, United Kingdom, CR3000 data logger, with a sensitivity of 10^{-4} °C and an absolute precision of 0.01 °C, regularly recalibrated. After 2014, an additional autonomous SB56 from Seabird™ with 10^{-3} °C accuracy and 10^{-4} °C resolution was installed to monitor temperature near the pathway in the RR (TRR in Fig. 1b). CDC was monitored with sensitivity of 0.01% (vol.) using sensor PIR7200 from Dräger™ sensors, Germany, intercompared twice a year, and recalibrated when necessary at each visit in the cave, with a high-precision portable Dräger™ sensor and an MX6 model from Industrial Scientific™, U.S.A., with an oxygen sensor. All CO_2 sensors were recalibrated in situ when necessary with standard gas references. Portable devices were also used to perform repetition profiles in the Chauvet cave along the pathways. Atmospheric pressure was recorded using a Vaisala™, Finland, PTB110 sensor with a sensitivity of 0.001 hPa. Relative humidity (RH) was measured from April 1999 to May 2000 in the Brunel Room with a chilled mirror sensor hygrometer from General Eastern™, USA, (model M4-type with high precision sensors), with 1% accuracy and 0.01% resolution.

Monitoring of biological germs in the cave air (Leplat et al., 2019) was also performed regularly at 18 points in the cave since 1997, using a Duo SAS Super 360 air sampler (VWR-pbi™, Milan, Italy). At each sampling point, 100 L of air was drawn through a 219-hole impactor containing appropriate culture media in 55 mm Petri dishes. The samples were then taken to the laboratory for analysis. Bacteria were isolated on nutrient agar (Merck KGaA, Darmstadt, Germany), and fungi were isolated on malt extract agar (Merck™, KGaA Darmstadt, Germany). The plates were incubated in a BD 115 incubator (Binder GmbH, Tuttlingen, Germany) at 30 °C for three days for bacteria, and at 24 °C for seven days for fungi. These incubation temperatures are higher than those found in the caves, and were chosen to allow rapid microbial growth. The number of microbial colonies grown in each Petri dish was counted after incubation time. Each count was corrected using the table of the most probable count, as recommended by the manufacturer. The results are expressed as colony-forming units per cubic meter (cfu m^{-3}).

The carbon isotopic ratio of gaseous CO_2, $\delta^{13}C$, expressed in ‰ relative to the standard values of Pee Dee belemnite (PDB), was determined from cave air sampled in glass tubes at three locations in the cave. CO_2 was extracted with cold traps, then analyzed using mass spectrometers at Orsay University and LSCE/Saclay, France. The two-sigma uncertainty on the $\delta^{13}C$ measurement was 0.1‰. In order to measure the ^{14}C activity of the cave atmosphere CO_2, we sampled 2 L of air in evacuated glass tanks. CO_2 was then extracted in the laboratory using liquid nitrogen and carbonic ice. CO_2 gas was then graphitized on iron with hydrogen at 600 °C for 3 h. ^{14}C atoms were counted on the ARTEMIS accelerator mass spectrometer (AMS) of the LMC14 national platform at CEA/Saclay (Dumoulin et al., 2017; Moreau et al., 2013).

3.2. Monitoring of water seepage and surface meteorological conditions

Cave water drip flow has been monitored continuously since 2013 at two locations named Cierge and Cactus (Fig. 1b), where permanent dripping takes place, and located in the vicinity of significant fractures (noted F in Fig. 1b). We used Stalagmate™ Plus Mk2b drip counters from Driptych (UK). This counter is a box, slightly larger than a 5 cm size cube, which records falling drop by its acoustic signal. Spurious response by noise (voices, cascading water) is rejected by the sensor (Chris Collister, www.driptych.com).

Surface meteorological data (temperature, atmospheric pressure and rainfall) are available at Aven d'Orgnac cave since 1997, and continuously since 1921 at the Montélimar meteorological observatory located 33 km north-east of Chauvet cave. Forest-scale CO_2 flux (Allard et al., 2008) has been monitored since 2000 in the Puéchabon climate observatory (PUECH) by the method of eddy covariance diffusivity (Fig. 1). Water excess (WE), which represents approximately the amount of infiltration water into the soil and then into the cave, is calculated by subtracting, from the monthly rainfall, the evapotranspiration calculated using the Thornwaite formula (Genty and Quinif, 1996). Additional meteorological data recorded in Vallon Pont-d'Arc, in the vicinity of the Chauvet cave, are also available after 1996.

4. General properties of Chauvet cave climate

4.1. Prior knowledge of thermal and natural ventilation regimes

Since 1997, the Chauvet cave has shown high thermal stability (Bourges et al., 2014a, 2014b) and RH close to 100%, with a mean value of 99.67 ± 0.01% from May 1999 to May 2000, and a peak-to-peak variation of 0.38% during this period. Mean air temperatures in the entrance debris cone (T0) and in the Brunel Room (T1) were 14.47 ± 0.01 °C and 13.89 ± 0.01 °C, respectively in 2017, while air temperatures were significantly lower (12.9 ± 0.01 to 13.0 ± 0.01 °C) in the Hillaire Room and the RR (Fig. 1b). The peak-to-peak amplitude of the annual variations was, in 2017, 2.2 °C in the entrance (T0) and 0.17 °C in the Brunel Room (T1). In the Hillaire Room and the RR, air temperature showed a high stability, with peak-to-peak ampli-

tude smaller than 30×10^{-3} °C, only affected by small transients due to atmospheric pressure variations, as expected for a confined location (Perrier et al., 2001, 2010; Bourges et al., 2006). These variations were of the order of 20×10^{-3} °C hPa^{-1} at a period of 4 h and were decreasing for longer periods, reaching 10^{-3} °C hPa^{-1} at a period of one week. Such variations, also present and similar in the atmosphere of the Brunel and Hillaire Rooms, and even in the more perturbed entrance T0, were smaller at the rock surface. Thermal perturbations due to human presence during the archaeological campaigns were clearly observed, with a relaxation of a few days (reaching weeks in the RR), as regularly noticed in underground conditions submitted to transient weak heating (Fernandez-Cortes et al., 2011; Crouzeix et al., 2006). Until now, no permanent irreversible thermal effect due to human intrusions, which have remained strictly limited in duration and quantity, has been detected in the Chauvet cave. Nevertheless, the RR appeared to be the most sensitive place to thermal accumulation.

Given the lack of large open access to the Chauvet cave, seasonal natural ventilation regimes can only be marginal. This was confirmed by a homogenous and stable radon-222 concentration of 7220 ± 250 Bq m^{-3}, with a yearly variation smaller than 10%. The main thermal condition observed in the cavity was stable thermal organization, with the colder layers at the bottom of the main rooms and in the RR. The main thermal forcing in the case of the Chauvet cave seems to be the solar heat dissipation on the steep cliff, essentially free of vegetation, due to its southern exposure (Fig. 1a). Consequently, the main thermal gradient in the Chauvet rock formation, and consequently the Chauvet air volumes, rather than being a vertically constrained stratification, may be horizontal along the south-north direction. Seasonal variations of the thermal stratification may also happen, competing with thermal diffusion through the encasing rock, a process that dominates only near the entrance. While mean air temperature was remarkably stable in the RR and in the Hillaire Room, slow and steady temperature evolution was observed in the rest of the cavity.

4.2. Infiltration and hydrogeological regimes

The water table is expected to remain well below the cave floor, at the level of the Ardèche river, flowing about 100 m lower. While flooding may always happen in a complex karstic context, the Chauvet cave is located at a relatively high altitude at the edge of the limestone cliff (Fig. 1a), and infiltrations are the only mode of water intrusion into the cavity. Water seepage explains the large speleothem development observed in the cave, currently active, but stopped during the coldest climate periods, such as the last glacial period between 22.3 ± 0.5 and 15.2 ± 0.5 ka BP (Genty, 2012; Genty et al., 2004, 2005).

The drip rates recorded in the cave show large differences and large temporal variations, from 10 drops per 15 min to above 1000 drops per 15 min during large infiltration transients that follow, with an irregular pattern, large rain events. These changing infiltration regimes reflect varying rainfall, monitored at Aven d'Orgnac (see inset in Fig. 1), and the varying saturation conditions of the vadose zone. The annual rainfall from the meteorological station in Orgnac was on average 922 ± 77 mm yr^{-1} (from 1997 to 2018), with significant year-to-year variability (1554.2 mm in 2014, 938.8 mm in 2015, 1100.0 mm in 2016, 536.0 mm in 2017, and 1570.6 mm in 2018). However, a particular feature to which we return below is the regular decrease of rainfall, from 2014 to 2017, during the spring-summer period (April 5 to September 5): 311.6 mm in 2014, 297.4 mm in 2015, 263.8 mm in 2016, 180.6 mm in 2017, but it was higher in 2018 (729.8 mm).

The oxygen isotopic composition ($\delta^{18}O$) of drip water from speleothems remained remarkably stable from 2000 to 2012, with an average of -6.89 ± 0.22‰. This indicates that the apparent mean residence time of water in the vadose zone above the cavity must be larger than several months to a few years (Genty et al., 2014), which is shorter than, for example, in the Villars cave in West of France (Genty, 2008). Nevertheless, faster transit times through localized episodic channels are likely to occur. The steady state and transient infiltrations should not have any significant effect on the thermal budget of the cavity. However, a significant effect, especially during transient infiltration, can be expected on the CO_2 input into the Chauvet cave, essentially through piston effects of CO_2-rich air from soil and rock layers.

5. Spatiotemporal patterns of CDC in the Chauvet cave atmosphere

5.1. Overview of CDC temporal variations

In contrast with the relative stability of air temperature, CDC displayed unexpected and unusual large temporal variations at the two monitoring locations in the Chauvet cave (Fig. 2a). Yearly parameters for CDC, in the Chauvet cave and in the reference caves, are listed in Table 1. In 2017, mean CDC was large at both locations (2.2% and 3.7% in A and B, respectively). CDC values larger than 3% are rarely observed in caves. For example, CDC did not exceed 0.5% in the Esparros cave (Fig. 2b), which is comparable with the Villars cave (Genty, 2008) or with other well ventilated sites such as mine tunnels or the Vincennes quarry near Paris, where CDC did not exceed 1% (Perrier and Richon, 2010). In the Pech Merle cave, CDC values were rather high, and varied around a mean value of 2% (Table 1). In the Aven d'Orgnac cave, CDC in the visited section did not exceed 2.9%, until June 2016, where it reached the maximum CDC threshold of 3% identified as the safety limit for visitors. Artificial ventilation that mimics the winter natural air circulation was then implemented and maintained permanently, resulting in a stationary low CDC in the visited section (Fig. 2b).

In the Chauvet cave, not only the mean CDC was large, but a quasi-sinusoidal yearly variation was also observed (Fig. 2), with the peak CDC exceeding 3.2% in A and 4.4% in B in 2017 (Table 1). While the yearly variation in B was almost sinusoidal, the variation in A showed successive linear periods with significant break points, except near its minima. The annual peak-to-peak amplitudes varied from 2015 to 2018, but remained slightly larger in A (1.5 to 2%) compared with B (1.5 to 1.7%). In the Esparros and Aven d'Orgnac caves, before 2016, the yearly cycle was dominated by strong seasonal ventilation during winter (Fig. 2b). In the Pech Merle cave, the seasonal natural ventilation regimes were modified by ventilation, artificially induced during visits of tourist groups (Bourges et al., 2014a). In addition, artificial remediation has been implemented by opening the entrance double door during dedicated periods, which reduced CDC in the visited section. Even in the absence of artificial action, in the Pech Merle cave and the upper sections of the Aven d'Orgnac cave, the maximum CDC in the visited section did not reach the levels regularly observed in the Chauvet cave. While a larger mean CDC was expected in the RR (at CO_2 B), a large annual variation was surprising and may have appeared, at first, incompatible with the confinement suggested by the temperature stability.

Not only CDC was large and peculiar in the Chauvet cave, but a clear increasing trend of CDC was revealed after 2013 (Fig. 2a). This behaviour was not observed in any of the reference caves (Table 1), except in the deep network of the Aven d'Orgnac cave, where speleological visits had to be cancelled after 2016. While CO_2 A also increased after 2013, the trend was particularly clear and continuous for CO_2 B, with spectacular yearly maxima of 3.85% in 2015, 4.13% in 2016, and 4.44% in 2017 (Table 1). The yearly minima of CO_2 B also increased similarly (Table 1). In contrast, the increase was less pronounced for the yearly minima of CO_2 A, and less continuous for the corresponding yearly maxima. When linear fitting is performed from October 15, 2014 to October 15, 2017 (Fig. 2a), we obtain a slope of $0.15 \pm 0.08\%$ yr^{-1} for A and $0.26 \pm 0.07\%$ yr^{-1} for B. This trend, however, did not continue in 2017 and 2018, since a decreasing

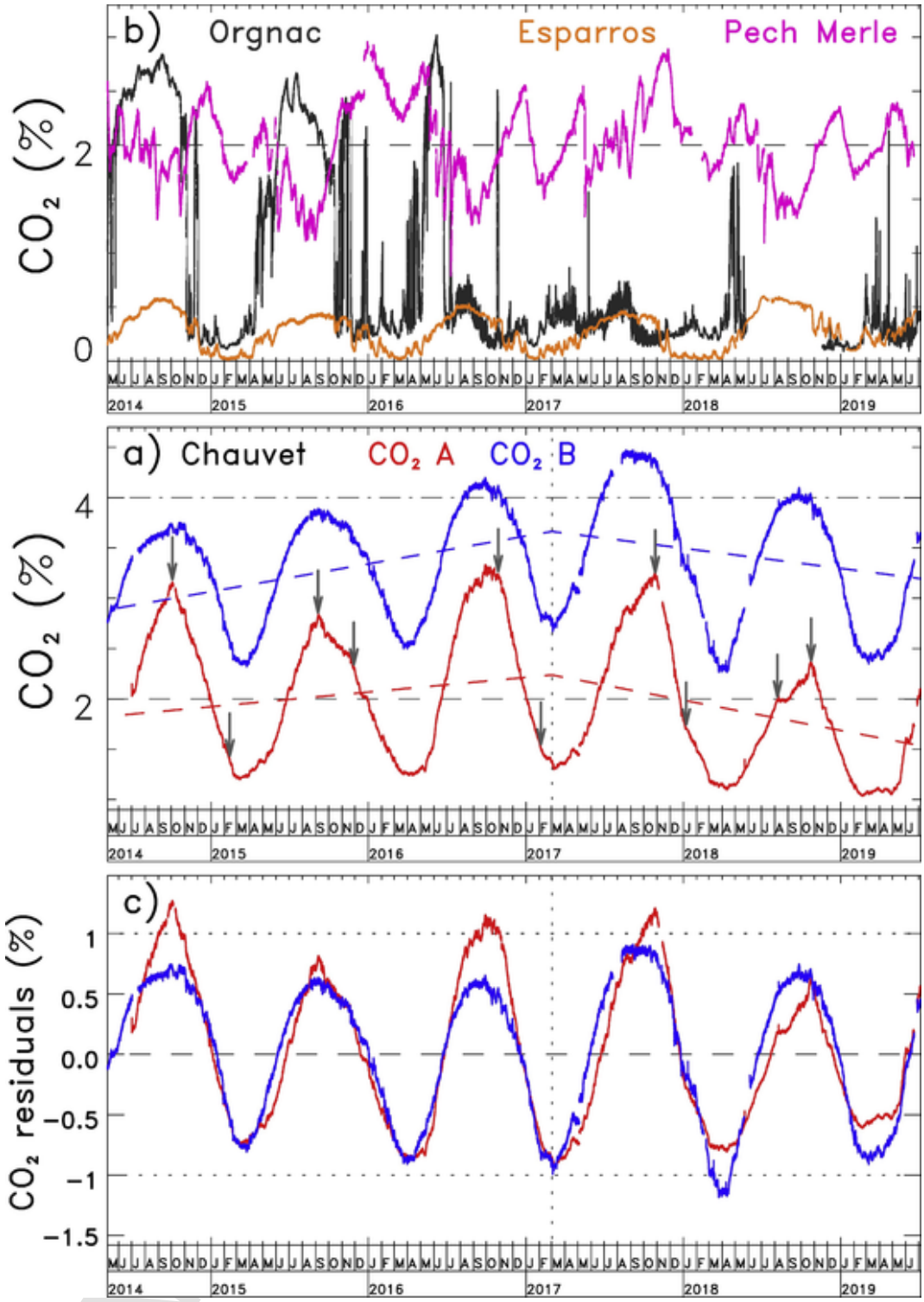

Fig. 2. a) Time-series of recorded CDC in the atmosphere of the Hillaire Room (A) and the Remote Room RR (B) of the Chauvet cave from 2014 to 2019. The grey arrows indicate some of the major break points in the evolution of CO_2 A. The dashed lines correspond to assumed long-term trends, which consist in a linear fit performed from January 1, 2014 to March 1, 2017, and a decreasing linear evolution afterwards. b) Corresponding CDC time-series recorded in the three reference caves: Esparros, Pech Merle, and Aven d'Orgnac. c) Corresponding time-series of CDC in the Chauvet cave (residuals) after subtracting the long-term trend (shown in a).

trend is observed after March 1, 2017, with a slope of −0.3 ± 0.05% yr^{-1} for A and − 0.2 ± 0.05% yr^{-1} for B. (Fig. 2a). When this long-term trend is subtracted, we can compare the annual variations of these residuals of A and B (Fig. 2c). On the average, the annual variations of the residuals appeared to be in phase (see Supp. Mat. S2).

5.2. Overview of CDC temporal variations since 1997 in relation with other parameters

A broader perspective is given when considering the complete data set since 1997 (Fig. 3). The values of CDC in 2017 were unprece-

Table 1
Overview of CO_2 concentration, expressed in % (vol.) in the atmosphere of the Chauvet cave and of three reference caves (Fig. 1) for the period from 2013 to 2018. For each year, the average concentration (arithmetic mean) with the minimum, maximum and annual amplitude of the time-series are given after averaging with a running window of 2 days. Values are not given for the Aven d'Orgnac cave after the implementation of an artificial ventilation scheme in 2016.

Location	CO_2 (% vol.)	2013	2014	2015	2016	2017	2018
Chauvet A	Mean CO_2 (%)			1.974 ± 0.003	2.201 ± 0.004	2.184 ± 0.003	1.654 ± 0.002
	Min-max-annual amplitude (%)			1.22-2.77-1.55	1.26-3.27-2.02	1.34-3.19-1.85	1.13-2.30-1.17
Chauvet B	Mean CO_2 (%)			3.244 ± 0.003	3.423 ± 0.003	3.697 ± 0.003	3.324 ± 0.003
	Min-max-annual amplitude (%)			2.36-3.85-1.49	2.54-4.13-1.58	2.76-4.44-1.68	2.31-4.02-1.72
Esparros	Mean CO_2 (%)	0.199 ± 0.001	0.288 ± 0.001	0.249 ± 0.001	0.254 ± 0.001	0.242 ± 0.001	0.314 ± 0.001
	Min-max-annual amplitude (%)	0.026-0.41-0.38	0.037-0.57-0.53	0.023-0.43-0.40	0.027-0.51-0.48	0.028-0.44-0.42	0.028-0.58-0.55
Pech Merle	Mean CO_2 (%)	1.833 ± 0.002	2.149 ± 0.002	1.891 ± 0.002	2.125 ± 0.002	2.119 ± 0.002	1.890 ± 0.002
	Min-max-annual amplitude (%)	1.27-2.57-1.3	1.65-2.6-0.95	1.25-2.86-1.6	1.35-2.87-1.52	1.64-2.28-1.19	1.40-2.32-0.92
Aven d'Orgnac	Mean CO_2 (%)	0.811 ± 0.004	1.426 ± 0.006	1.264 ± 0.005	0.705 ± 0.004		
	Min-max-annual amplitude (%)	0.11-1.93-1.82	0.12-2.78-2.66	0.13-2.52-2.39			

dented. While CDC values at B larger than 4% have been observed before in 2008 and in 2009, they have not persisted, and have not been accompanied with a simultaneous larger CDC in A. CDC, in contrast, has been relatively stable before 2007, and CO_2 B did not exceed 3.3%. The temporal evolution of CDC in the Chauvet cave from 1997 to 2017 followed the T1 temperatures in the Brunel Room (Fig. 3b), which, incidentally, also displayed an anomalous and regular increase from 2012 to 2017. However, such temperature increase did not appear to be systematically related to the evolution of the outside temperature in Orgnac (Fig. 3e). Furthermore, the yearly amplitude in temperature T1 was not clearly following the yearly amplitude of CO_2 A or CO_2 B (see Supp. Mat. Fig. S3–4).

An independent view on the conditions in the Chauvet cave is given by the monitoring of microorganisms (Fig. 3c). The location of the 18 sampling points is shown in Supp. Mat. Fig. S5. Mean concentrations, 289 ± 31 cfu m^{-3} for bacterial germs and 80 ± 11 cfu m^{-3} for fungal germs, were rather low compared with the concentrations in other caves monitored in a similar fashion (Leplat et al., 2019). This can be expected in an isolated cave where biological nutrients are rare and access is restricted. The largest mean bacterial (478 ± 157 cfu m^{-3}) and fungal (213 ± 108 cfu m^{-3}) concentrations were not observed near the entrance, but in the Megaceros Corridor. Increase of bacterial concentration near the end of caves has been reported in other cases, but was not associated with a fungal concentration increase (Leplat et al., 2019). When the values from the points inside a same large chamber were averaged (Fig. 3c), spatial variations appeared small compared with temporal variations. Comparatively, larger fungal concentration observed in 2013 returned to previous low 2004 level within a few months. Thus, the trends observed from the monitoring of germs in the Chauvet cave were not related to the global changes of underground conditions revealed by CDC (Fig. 3a) and temperature data (Fig. 3b).

The CDC temporal variations observed in the Chauvet cave (Fig. 3a,b,c) did not follow the evolution of the CDC in the outside atmosphere, as reflected by the steady variations of atmospheric CDC in PUY and OHP (Fig. 3d), or of the regional CO_2 flux at forest scale recorded in PUECH (Fig. 3d), which was characterized by a significant evolution of its seasonal modulation (Rodriguez-Calcerrada et al., 2014). Other time-varying surface forcings are surface atmospheric temperature (Fig. 3e) and rainfall (Fig. 3f). The surface meteorological forcing displayed little variations from Orgnac (7 km from Chauvet) to Montélimar (33 km from Chauvet), and thus can be considered regional rather than local.

5.3. Spatial structure of CDC versus time

In addition to the two locations A and B measured continuously, CDC was also repeatedly measured at reference locations along the pathway from the entrance to the end of the RR (Supp. Mat. Fig. S6). The highest CDC values have been systematically associated with a decrease of oxygen concentration. To separate the spatial variations from the temporal variations, dominated by the seasonal variations, the obtained CDC profiles were normalized to the value measured in location A (Fig. 4). The CDC clearly remained remarkably uniform in two main compartments: the large domain comprising the Brunel and Hillaire Rooms, where sensor A is located, and the RR, where sensor B is located. Some sub-compartments may be distinguished within the main compartment, with a slightly more variable zone in the Brunel Room, and a zone with a small systematic CDC increase between the Bauges and Hillaire Rooms. In two transitional domains (the entrance zone and the Megaceros Corridor leading to the RR), CDC was more variable. In winter, the transition zone was sometimes wider than a few meters in the entrance tunnel and sometimes rather abrupt within one meter, whereas the transition was from 2 to 3 m wide in the Megaceros Corridor. In summer, transitions are narrower, of the order of a few decimeters, in the entrance conduit and the Megaceros Corridor. In the latter, it is located at the topographic high of the slope down to the RR. When radon concentration is measured simultaneously with the CO_2 profile (inset of Fig. 4), homogeneous values are also observed from the Brunel Room to the Hillaire Room, with only a 10% increase at the entrance of the RR, where CDC is increased by 65%.

The variations in CDC along the profile did not reflect a horizontal stratification. Indeed, when considering CDC values versus the altitude in the cave along the pathway (Supp. Mat. Fig. S7), no variations were observed in a given compartment. In a given room, for all available time periods, CDC was homogeneous over a height of 3 to 6 m, larger than the mean altitude difference between A and B across the Megaceros Corridor. Thus, vertical CO_2 stratification, observed in some cases (Choppy, 1965), is completely ruled out in the case of the Chauvet cave, where horizontal large-scale organization prevails.

5.4. CDC and natural ventilation

The temporal variations of CDC cannot be attributed to natural ventilation or seasonal mixing with outside atmosphere driven by temperature variations. In purely horizontal systems, the ventilation rate is basically constant throughout the year (Richon et al., 2005). In a dead-end system with opening above, cold air enters the underground cavity when the outside air density is larger than the mean density in the cavity (Perrier et al., 2002). When outside air enters the cavity, CDC is suddenly reduced to small values, as confirmed in the Aven d'Orgnac cave (Fig. 5a). The CDC then returns to typical cave values as soon as the outside temperature increases again (Fig. 5). Therefore, such effect leads to a specific temporal pattern with large and rapid variations, common in all similar systems, such as the Esparros cave or the Vin-

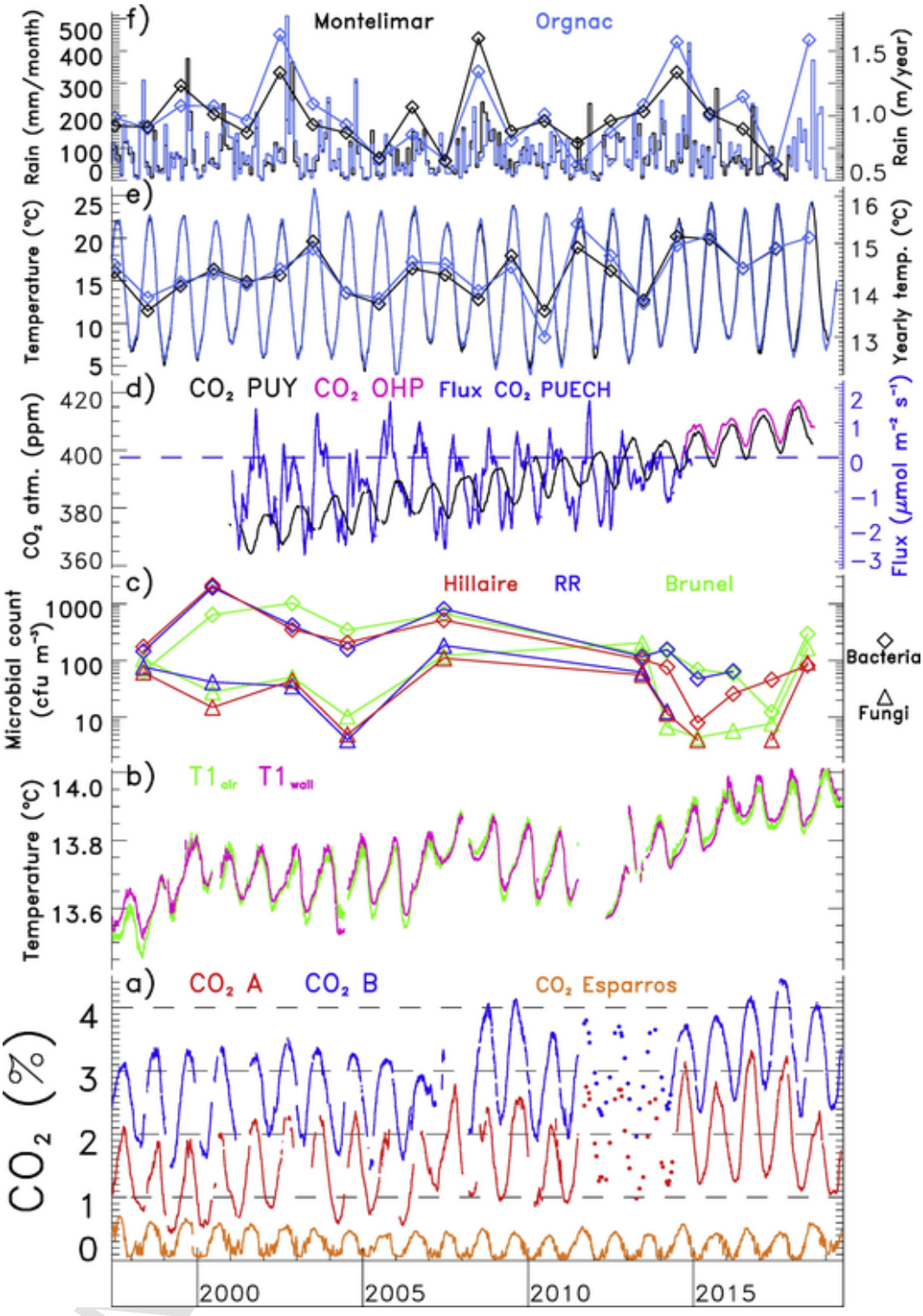

Fig. 3. Long-term overview of environmental conditions in the Chauvet cave: a) Daily values of CDC in the Chauvet and Esparros caves from 1997 to 2019. Values obtained in the Chauvet cave during the regular maintenance inspections are used when the recording system was not functioning from 2011 to 2013. b) Daily values of temperature recorded in the Brunel Room of the Chauvet cave (T1), in the air and at the wall. c) Mean microbial count expressed in colony-forming units per cubic meter of air, separately for bacteria and fungi. The data from various points available in the main rooms are averaged (see Supp. Mat. Fig. S5). d) CDC in the atmosphere measured in the PUY and OHP observatories (left scale). In addition, the CO_2 flux to the atmosphere measured from eddy covariance diffusivity in PUECH is shown (scale on the right hand side). e) Mean daily temperature at Orgnac and at Montélimar, presented with a running average of 90 days length. The mean yearly temperatures at the two locations are shown with the scale on the right hand side. f) Monthly rainfall at Orgnac and at Montélimar. The yearly rainfall at the two locations is shown with the scale on the right hand side.

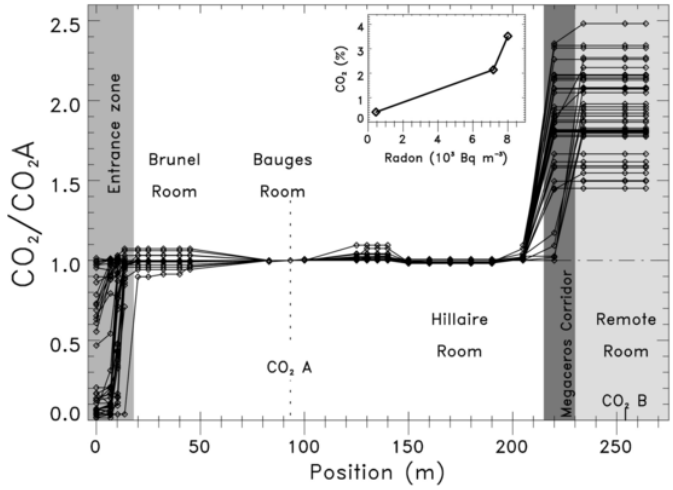

Fig. 4. Ratio of CDC to the CDC in the Chauvet cave at the reference point A along the pathway from the entrance to the end of the RR, obtained during the regular maintenance visits in the cave. The locations of the permanent measurement points A and B are indicated above the horizontal scale. CDC is shown in inset versus radon concentration as measured along a profile from the entrance to the beginning of the RR carried out on July 4, 2019.

cennes quarry near Paris (Perrier and Richon, 2010). Such a temporal variation is excluded in the Chauvet cave, where the moments of the mean values of CDC do not coincide with the moments of the year when the air densities outside and inside the cave are equal.

Furthermore, when natural ventilation occurs, radon concentration behaves in the same manner as CDC (Perrier and Richon, 2010; Bourges et al., 2006). This is not observed in the Chauvet cave (Fig. 5a), where radon concentration is rather constant throughout the year, not matching the CDC variation. The radon concentration shows only a possible 10% increase during the summer months, unlikely to be attributed to a thermal ventilation effect driven by the outside temperature, the required temperatures being then largely above the mean cave temperatures. The decoupling between radon and CDC, also mentioned previously for the spatial variation, unambiguously rules out a temporal variation of CDC induced by mixing with outside atmosphere. In addition, if a reduction of CDC would be due to an input of outside air into the cave, this would have been revealed by the presence of biological germs, especially during the spring. The stability of the biological cleanliness of the Chauvet cave air (Fig. 3) also supports an atmospheric confinement of the cave. Natural ventilation in any case could not be expected to produce a large effect because of the presence of doors (Fig. 1). Only leakage through the debris cone obstructing the natural entrance and possibly through the aperture under the climatic door (4 cm × 60 cm) remains possible. Radon concentration suggests that such leakage, if present, cannot modify cavity air parameters by >10%.

5.5. Carbon isotopic composition of Chauvet cave CO_2

The carbon isotopic composition of CO_2 in the Chauvet cave atmosphere was measured at 3 locations at various times (Fig. 6). The carbon isotopic composition appeared stable through time, with a mean $\delta^{13}C$ value of −23.3 ± 0.2‰ (n = 17), similar to the mean value of −23.0 ± 0.2‰ (n = 4) reported in the Lascaux cave (Houillon et al., 2017), or the mean value of −22.5 ± 0.45‰ in the Villars cave from an extensive data set (n = 71) (Genty, 2008). In the Cussac cave (Dordogne, France), a mean value of −23.3 ± 0.35‰ (n = 7) was reported from 2009 to 2014. These $\delta^{13}C$ values also coincide with

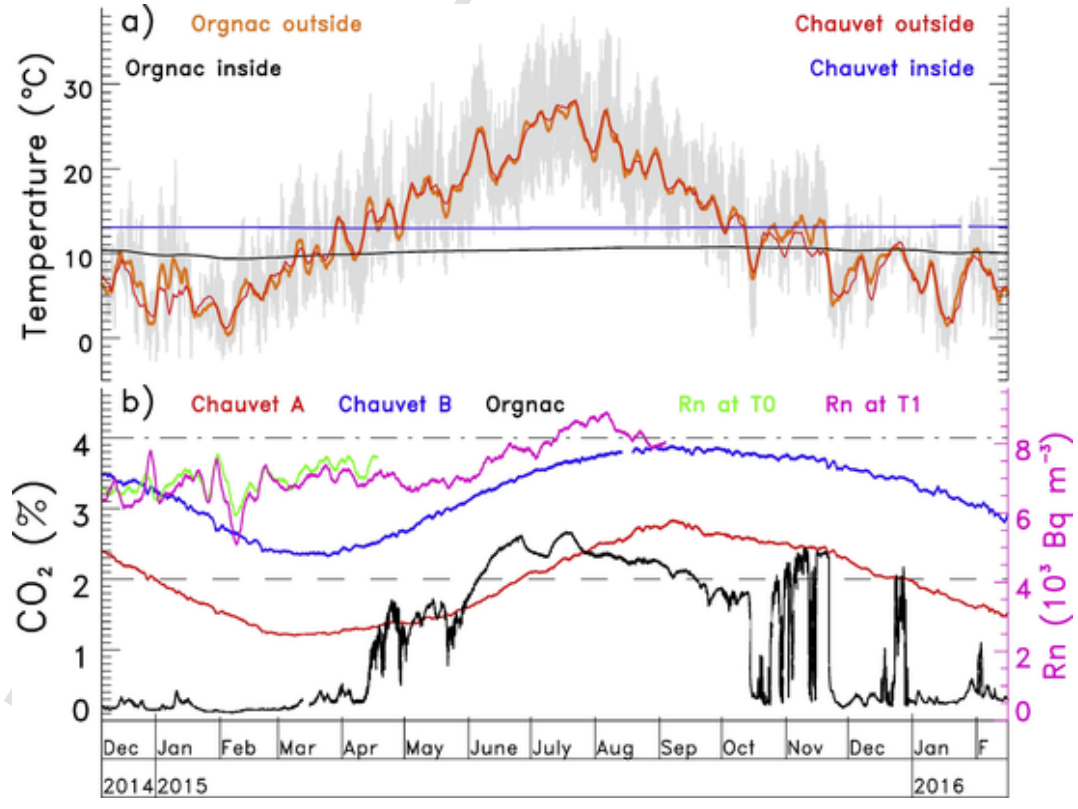

Fig. 5. Comparison between the Chauvet confined cave and the Aven d'Orgnac open pit cave: a) Outside temperature in Orgnac (grey curve) and Vallon Pont d'Arc, with a running window of 4 days duration (orange and red curves for Orgnac and Vallon Pont d'Arc, respectively), compared with the temperature inside the Aven d'Orgnac cave (black curve) and Chauvet cave (blue curve). The cave temperatures, recorded in saturated conditions, were corrected to correspond to the mean RH recorded outside. The outside and inside temperatures cross when the air densities outside and inside are equal. (For interpretation of the references to colour in this figure legend, the reader is referred to the web version of this article.)

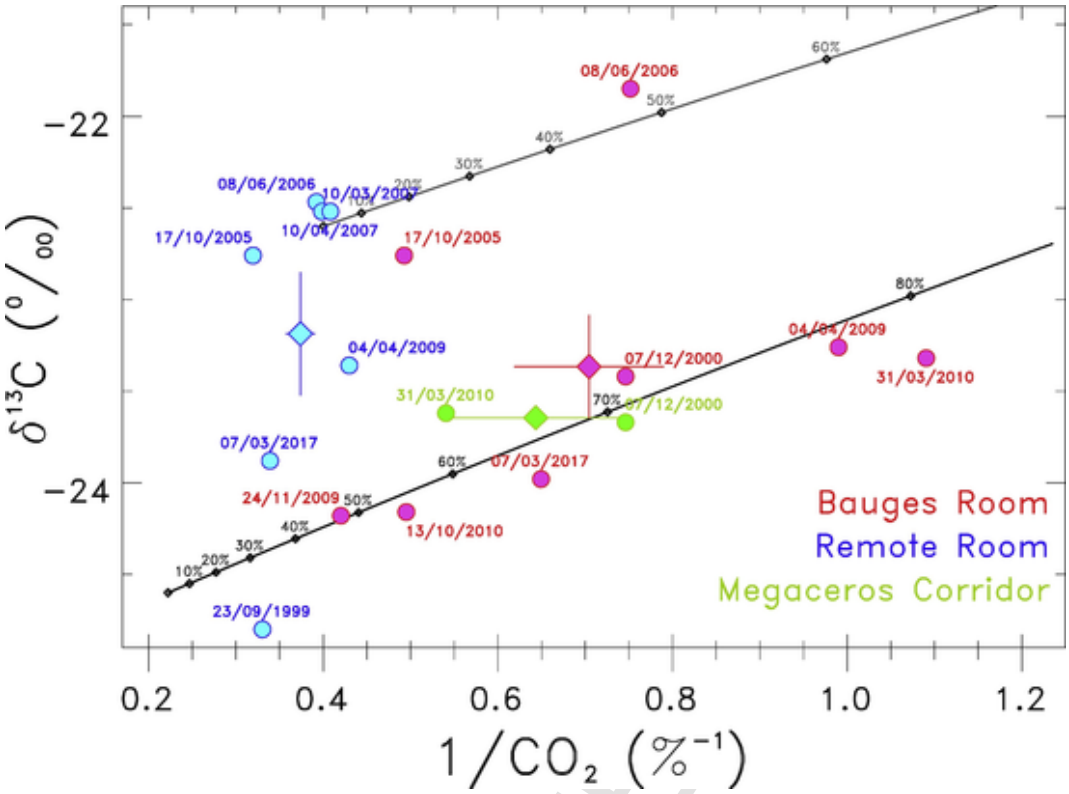

Fig. 6. Carbon isotopic ratio ($\delta^{13}C$) of atmospheric CO_2 as a function of the inverse of CDC expressed in $\%^{-1}$ for three locations in the Chauvet cave. Circles show the data points and diamonds the averages for each location. The lines refer to mixing models between one internal pole (4.5%, −22.6‰ or 4.5%, −24.6‰) and the outside atmosphere (0.04%, −8.5‰), with the volume fraction of outside atmosphere along the mixing lines indicated in %.

the smallest values reported in deep Gibraltar karst (Mattey et al., 2016), a rather different type of underground system.

At the Chauvet cave, no clear relationship emerged between $\delta^{13}C$ and CDC (Fig. 6), unlike what was observed in other caves such as the Villars cave, for example, where $\delta^{13}C$ decreases when CDC increases (Genty, 2008). While the mean CDC values are different, the mean values in the different compartments were remarkably similar: −23.36 ± 0.28‰ (n = 8) in the Bauges Room, −23.19 ± 0.33‰ (n = 7) in the RR, and − 23.65 ± 0.03‰ (n = 2) in the Megaceros Corridor. These values are also consistent with $\delta^{13}C$ values associated with the highest CDC in other caves in the South of France. Thus, at the Chauvet cave, the temporal $\delta^{13}C$ changes remained small around a value likely to be close to the minimum value found in underground systems and larger than the typical values found in soils. Some locations appeared more stable with time than others, and larger $\delta^{13}C$ values were measured between 2005 and 2007 (Supp. Mat. Fig. S8), followed by an overall decreasing trend. The temporal variations were generally small, but were significant in comparison with the measurement uncertainty (0.01 to 0.03‰).

Mixing with atmospheric air (Fig. 6) does not account for the observed temporal variations, especially for CO_2 B, but also for CO_2 A. However, the point representing the average value of $\delta^{13}C$ for CO_2 A is compatible with some average mixing with atmospheric air. Thus, while temporal variations cannot be interpreted by changes in atmospheric air content, static mixing can explain the lower average value of CDC in compartment A. To account for the varying values of $\delta^{13}C$, several CO_2 sources in the Chauvet cave must be present, in accordance with previous studies performed at other locations (Mattey et al., 2016; Genty, 2008). One end-member is characterized by $\delta^{13}C$ around −24‰ and another end-member with a larger $\delta^{13}C$, possibly greater than −20‰, associated with a lower equilibrium CDC. These possible two end-members could correspond to two distinct GC sources, rather than SC.

More than long-term variations, temporal variations appeared more organized according to the time of the year (Supp. Mat. Fig. S9): a coherent increase was observed from January to June, followed by a decrease and lower values from September to December, suggesting the dominance of a seasonal cycle. However, the number of data (n = 17) is not sufficient to be able to draw firm conclusions on this basis alone.

The $\delta^{13}C$ data are further complemented by ^{14}C data (Table 2). Since the first measurements, in 1999, we have observed a decreasing trend in the ^{14}C activity of all the stations of about −4 pMC, which corresponds to a gradient of about 2 pMC over 10 years, following the observed atmospheric decreasing trend. The difference between the ^{14}C activity in the cave and the ^{14}C activity in the outside atmosphere has also decreased over the past 20 years: it was about −3 pMC in 1999 and − 4 pMC in 2017. A synthesis of the available data (Table 1) indicates that the main frontal part of the cave (Bauges Room) in 2017 shows a ^{14}C activity 4 pMC lower than that of the atmosphere, and that the RR shows a ^{14}C activity 2 pMC lower than that of the Bauges Room. Thus, we suggest that the source of the CO_2 in the deepest part of the cave (RR) is, on the average, made of older CO_2, due to the decomposition of older SOM. The Bauges Room has a 2 pMC higher ^{14}

Table 2
Summary of CO_2 isotopic composition analyzed simultaneously with ^{14}C activity in the Chauvet cave and comparison with the outside atmosphere. Uncertainties include measurement uncertainties; pMC stands for percent Modern Carbon.

Quantity	Bauges Room	Remote Room	Outside atmosphere
$\delta^{13}C$ (‰)	−23.58 ± 0.05	−23.19 ± 0.05	−8.00 ± 0.05
^{14}C activity (pMC)	102.9 ± 0.2	100.9 ± 0.2	107.0 ± 0.2
CDC (ppm vol.)	15,180 ± 10	27,500 ± 10	350 ± 10

C activity, not because of a higher atmospheric component, but more likely because of a more recent SOM source or a more important part of bomb-contaminated SOM.

5.6. Spectral content and apparent barometric effect

The frequency content of CDC in the Chauvet cave appeared significantly different compared with that of the reference sites (Fig. 7). Fourier amplitude spectra of CDC in the Chauvet cave showed a large semi-diurnal peak S2, significantly larger than the diurnal peak S1, barely visible in the case of CO_2 A. A significant peak at 8 h also emerged clearly. In contrast, CDC in the Esparros, Aven d'Orgnac, and Pech Merle caves exhibited the opposite behaviour, with a dominant S1 peak. No significant earth-tide peak M2 can be identified above the continuum level in any of the underground sites.

Dominance of the S2 peak indicates sensitivity to atmospheric pressure variations, while dominance of the S1 peak reveals diurnal temperature or human effects (Perrier and Richon, 2010; Richon et al., 2009). For example, the S1 peak in the Pech Merle cave reflects CO_2 human breathing during visits and transient air motions due to door openings. Dominance of S1 peak is compatible with the fact that the Esparros, Aven d'Orgnac and Pech Merle caves are affected by large natural ventilation effects which exhibit characteristic large daily and seasonal variations (Fernandez-Cortes et al., 2009; Batiot-Guilhe et al., 2007; Perrier et al., 2007). The presence of a signature of atmospheric pressure variations in CDC, however, is not necessarily reasonable in a confined cavity such as the Chauvet cave, especially in the RR where the effect is the largest. Instead, the apparent pressure sensitivity, obvious in the time-series (Fig. 8a), results from an often overlooked instrumental artefact. Indeed, conversion of IR adsorption to CDC value C is sensitive to atmospheric pressure p, which is not corrected dynamically, causing a relative coupling $(\Delta C/C)/p$ of 0.15% hPa^{-1}, particularly visible at the Chauvet cave where the mean concentration, C, is unusually large (Supp. Mat. Fig. S10).

After applying the necessary instrumental correction factor, only small residual variations are observed (Fig. 8b), even smaller at other times (Supp. Mat. Fig. S11); the peaks completely vanish from the amplitude spectra (Fig. 8c). The fact that no diurnal variations remain, in both CO_2 A and B, also supports the previous conclusion on the absence of natural ventilation effects in the Chauvet cave. The corrected CDC appeared particularly stable in the B compartment (Fig. 8b and Supp. Mat. Fig. S11), whereas transient variations appeared clearly in the A compartment, suggesting that another process controls CDC in the Chauvet cave.

6. Infiltration, seepage and CDC in the Chauvet cave

6.1. Monitoring of seepage in the Chauvet cave and mid-term CDC temporal variations

A significant clue on the origin of temporal CDC variations was identified when considering the drip counter data (Fig. 9), focusing on the 2014–2018 period when high resolution data are available almost continuously. In this figure, the drip counts, recorded with 10 min sampling interval before 2017 and 15 min interval after 2017, were converted to a homogenous time interval of 30 min. The drip count data from the two locations, separated by about 45 m, showed sometimes significant differences (Fig. 9c), but, most of the time, the temporal variations, spanning over two orders of magnitude, were remarkably similar at the two locations, simultaneous at long timescales. At timescales smaller than one day, the two drip counts were less synchronous. Low drip counts are observed in the summer, and sudden inputs were regularly observed in fall and winter. While peak seepage discharges seemed similar over the time period considered in Fig. 9, the base level appeared to have continuously increased with time, an effect that cannot be attributed to spurious displacements of the sensors,

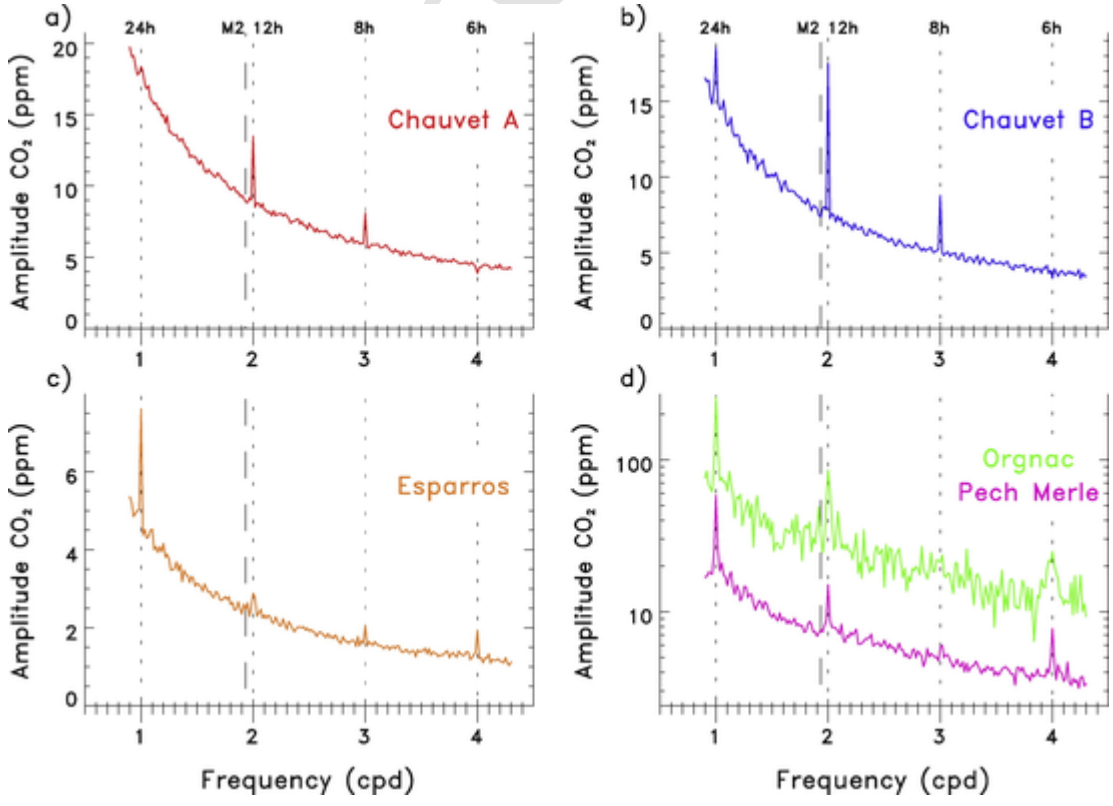

Fig. 7. Fourier amplitude spectra as a function of frequency, expressed in cycles per day (cpd), of a) CDC in the Chauvet cave A compartment, b) CDC in the Chauvet cave B compartment, c) CDC in the Esparros cave, and d) CDC in the Pech-Merle and Aven d'Orgnac caves.

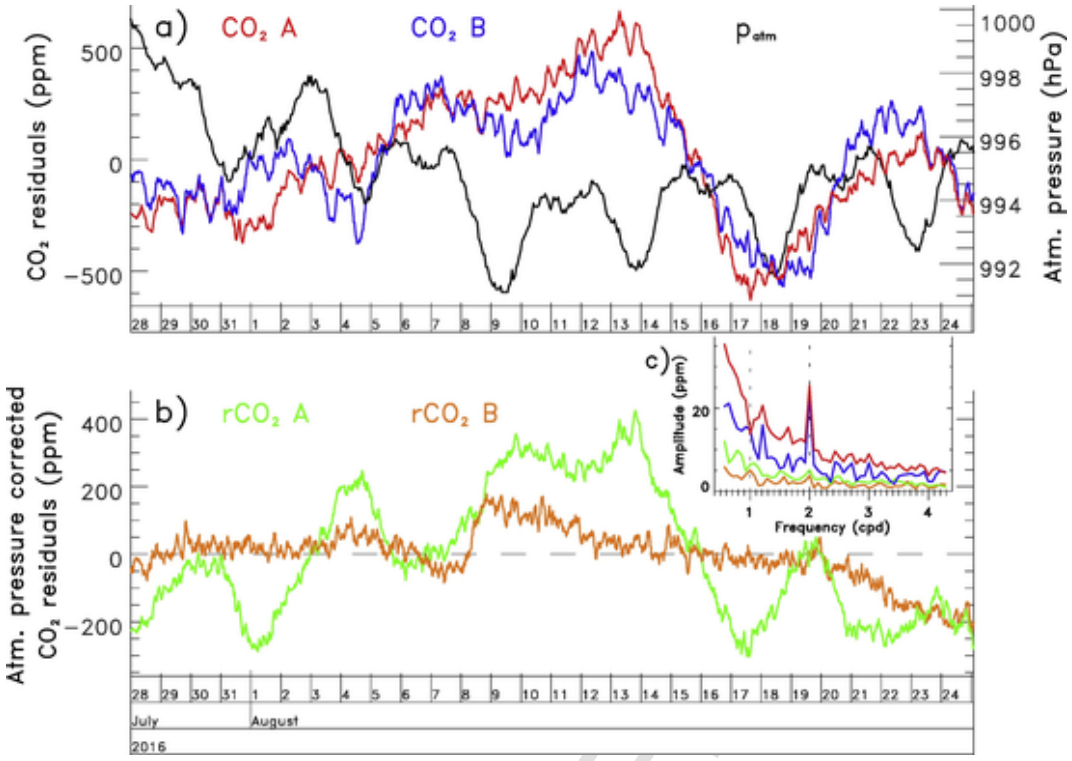

Fig. 8. a) Time-series of CDC residuals in the Chauvet cave, obtained by subtracting the seasonal trend given by a polynomial fit for the corresponding time section. The corresponding time-series for atmospheric pressure is shown in black with the scale given on the right hand side. b) Corresponding time-series of CDC residuals, corrected for the effect of atmospheric pressure on the CO_2 recording instrument (see text). c) Comparison of the amplitude spectra of CDC before and after correction for the atmospheric pressure effect.

and was similar at both locations. The peak discharge remarkably followed rain episodes shown in Fig. 9d. Furthermore, the seepage events, measured locally under centimetric dripping points in the Chauvet cave, are clearly associated with water level increase in the Orgnac borehole, where a large-scale aquifer is sampled, 7 km from the Chauvet cave. The infiltration episodes, thus, are not only homogeneous at the scale of the Chauvet cave, but are regional events in the karst formations.

A clear relationship emerged between the drip count (Fig. 9c) and CDC time-series (Fig. 9b). A sudden decrease of CDC from the maximum level was associated with the onset of large seepage events, an effect particularly clear with CO_2 A, but also visible with CO_2 B. Conversely, CDC increased regularly during the decreasing period of seepage, from April/May to August. Smooth sections of CDC, in general, corresponded in Fig. 9 to smooth decreasing variations of drip count (for example June to August 2015 or 2018), while rapid negative changes of slope in CDC corresponded to the onset of water flow. The calculated WE confirms this observation (Fig. 9d), with large WE systematically obtained during seepage events, and water deficits, taken as 0 when WE was negative in the calculation, systematically associated with increases of CDC. Rain events occurring during the water deficit period (for example the summer months of 2016 and 2017 in Fig. 10), are not associated, as expected, with seepage in the cave. The onset of water excess is a better predictor of CDC reductions than the drip flow. Indeed, when considering the section from May 2017 to September 2018 (Fig. 9 and, with an expanded timescale, Supp. Mat. Fig. S12), the beginning of the fast reduction of CO_2 A (beginning of November 2017) does not correspond to measured drip flow at Cierge point, but coincides with the onset of water excess evaluated from the surface. This fact indicates that the process controlling CDC is not the water flow itself, but the hydrogeological condition in the rock and soil above the cavity.

Temperature in the Chauvet cave was also affected by water discharge events. This effect was particularly clear with temperature T0 in the debris cone (Fig. 9b), with sudden negative change of slope similar to the effect on CO_2 A, particularly clear in September 2015 or November 2017, but slightly different in September 2017. The seasonal cycle of T0 followed the seasonal cycle of CDC by one to two months. The sudden onset of water discharge was also associated with a positive change in temperature T1 in the Brunel Room (Fig. 9a), while no clear change was observed in the RR, with TRR remaining remarkably stable within 0.02 °C over the 4 year period. Such sudden changes in temperature cannot occur from temperature diffusion effects at depth, but can result from advection. In the Chauvet cave, water discharge therefore largely controls the intermediate timescale variations of temperature T0, with a negative correlation, whereas a smaller but significant effect is produced on temperature T1, with a positive correlation. Not only was the atmosphere temperature affected in T1, but the wall temperature as well. No influence was identified so far on TRR.

Consequently, the data unambiguously indicate that the CDC seasonal cycle in the Chauvet cave was associated with the seasonal hydrogeological infiltration regime, with large sudden seepage event following rainfall with a time scale of a few days maximum, followed by smooth relaxations of a few months duration. Therefore, two timescales control infiltration: a long timescale of a few months, probably associated with drainage and capillary adsorption in the bedrock porosity, and a short timescale of the order of a few hours to two days, probably associated with fast drainage through large connected fractures.

6.2. Long-term relationship between WE and CDC

The relationship between the CDC cycle and the hydrological seasonal cycle was also observed when considering the whole data set from 1997. Drip count data were only available after 2011 (Supp. Mat. Fig. S13). The onset of CDC reduction always corresponded to the beginning of the water excess season (Fig. 10), which corresponded to water infiltration into the cavity, in most cases, and, with a delayed re-

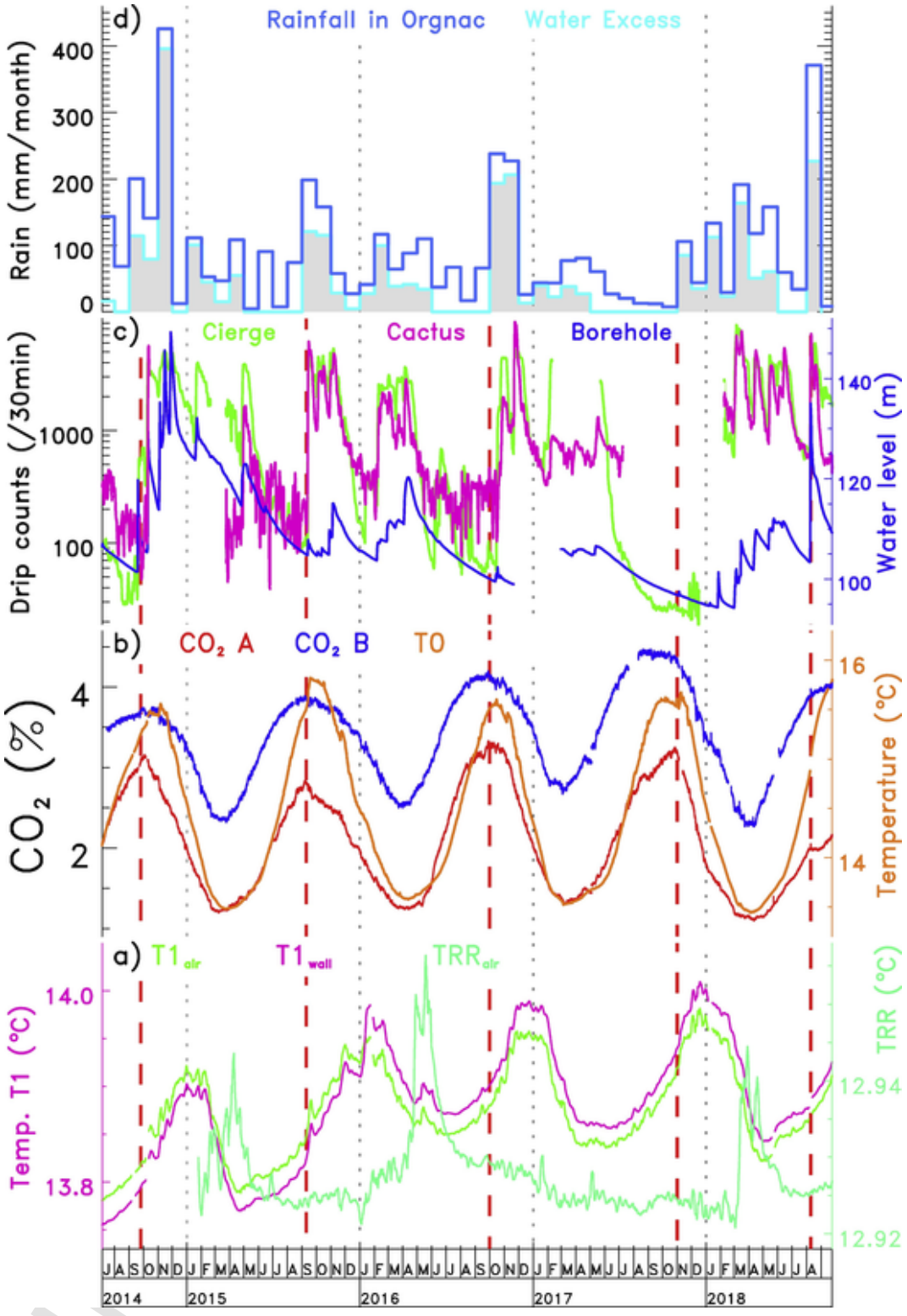

Fig. 9. Overview of the effect of infiltration into the Chauvet cave from 2014 to 2019: a) Air and wall temperatures in the Brunel Room (T1, scale on the left) and air temperature in the Remote Room (TRR, scale on the right). Time-series with 15 min sampling interval are averaged with a running window of 12 h. b) CDC in the Chauvet cave (locations A and B, left scale) and temperature in the entrance debris (T0, right scale). c) Drip counts at Cierge and at Cactus (see Fig. 1b, left scale) and daily values of water level in the Orgnac borehole (right scale). The drip counts, converted to a homogeneous sampling interval of 30 min, are filtered with a running window of 12 h. d) Monthly rainfall and calculated Water Excess in Orgnac. The vertical dashed red lines refer to the change from water deficit to water excess conditions, systematically associated with CDC reduction. (For interpretation of the references to colour in this figure legend, the reader is referred to the web version of this article.)

sponse to the water level in the Orgnac borehole. Furthermore, the water deficit periods did coincide, over the whole 1997–2018 period, with the seasonal increase of CDC. The mid-term slow variations of CDC, over 4 to 5 years, however, were not systematically associated with a similar trend in water level or WE. Indeed, the CDC increase observed from 2014 to 2017 was related to both a longer period of small

WE

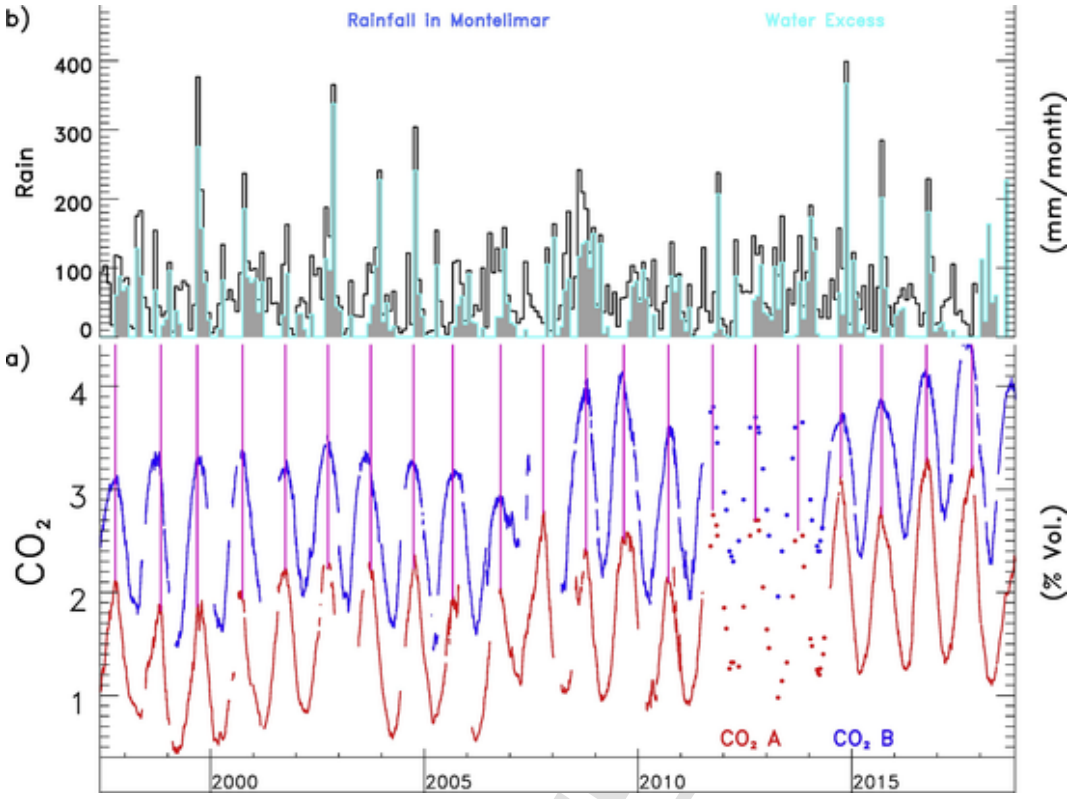

Fig. 10. Overview of the effect of infiltration on the CDC in the Chauvet cave from 1997 to 2019: a) CDC in the Chauvet cave. b) Monthly rainfall and calculated Water Excess at Montélimar. The vertical purple lines indicate the seasonal change from water deficit to water excess conditions, systematically associated with CDC reduction. (For interpretation of the references to colour in this figure legend, the reader is referred to the web version of this article.)

and longer summers with water deficit. Whereas the decrease from 2008 to 2010 was associated with both a larger WE and a shorter water deficit season, a similar correlation is not observed from 2004 to 2008. From 1997 to 2002, a period of larger WE (2000 to 2002) followed a period of smaller WE (1997 to 1999), but mean CDC and seasonal amplitudes remained stable from 1997 to 2002, irrespective of the mid-term variations in the hydrogeological forcing. Thus, a relationship between infiltration and CDC is not systematic at the inter-annual scale and not clear for long-term trends (Supp. Mat. Fig. S14). When present, it appears strongly non-linear, possibly dependent on the past history. This suggests that long-term CDC variations are controlled by another effect, such as changes in vegetation density above the cave, due to cessation of pastoral activities. The latter must have increased the SOM source and the soil CO_2 production (more roots and more micro-organisms), in addition to the evapotranspiration which affects the infiltration pattern, and then CDC in the cave. In addition, the increase of outside temperature may also have contributed further to a higher CO_2. Modifications of the aerological conditions in the entrance tunnel before 2004, might also have played a role.

The $\delta^{13}C$ data confirmed the dominant control of seepage on the cave air CO_2. While $\delta^{13}C$ was not clearly associated with CDC (Fig. 6), in contrast with sites such as the Villars cave having a broader range of CDC values (Genty, 2008), a clearly negative correlation is revealed as a function of WE (Fig. 11), with a correlation coefficient of −0.77 (n = 17). In Fig. 11, negative values of WE (water deficit domain) are also included, with WE during the fall season associated with the smallest $\delta^{13}C$ values and with water deficit during the spring and summer seasons associated with the largest $\delta^{13}C$ values. Despite the low temporal resolution of the cave air sampling, we observed that: 1) the $\delta^{13}C$ of CO_2 in the cave exhibits lower values in the fall (with a minimum in October), when the CDC is at its maximum and WE has just increased; 2) the $\delta^{13}C$ of CO_2 in the cave is at its maximum when CDC is at its minimum in early spring. The seasonal variations suggested in the time-series (Supp. Mat. Fig. S9) reflects the seasonal variations of the hydrological cycle.

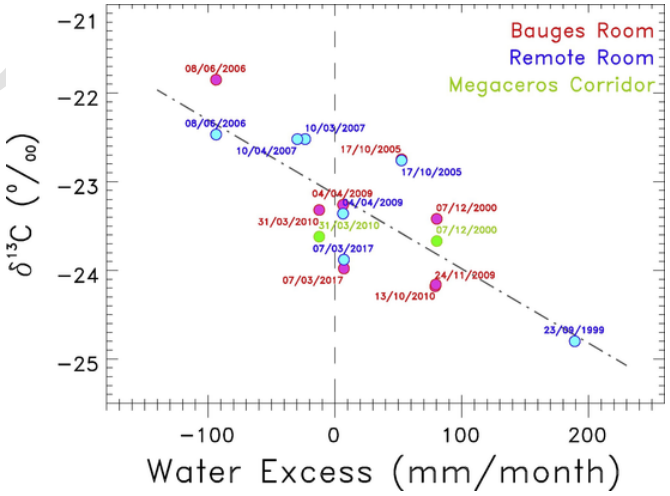

Fig. 11. Carbon isotopic ratio $\delta^{13}C$ of atmospheric CO_2 versus calculated Water Excess in Montélimar. The dash-dot line represents the fitted linear trend, which has a slope of −0.0084‰/(mm/month).

7. Discussion and interpretation

From the observations presented above, conclusions can be drawn on the origin of CO_2 and its transport modes into the Chauvet cave. While alternative interpretations are possible, a model is proposed as a reliable basis for future detailed modelling.

7.1. Seepage as control of temperature variations

The short-term temporal variations of CDC and of some cave temperature, with timescales smaller than a few months, were mainly controlled by the seepage regimes. Concerning the pluri-annual variations and long-term trends, different conclusions emerged for CDC and temperatures.

For temperature T1, the observed long-term trend can be explained by surface warming. When considering only thermal diffusion, the temperature time-series at a given depth can be calculated analytically for one-dimensional heat penetration in a stratified half-space (Perrier et al., 2005a). Assuming a homogeneous half-space with a thermal diffusivity of 10^{-6} m^2 s^{-1}, the measured T1 time-series is compared in Fig. 12 with the calculated time-series at various depths, taking the atmospheric temperature time-series recorded at the Montélimar observatory (Fig. 12a) as boundary condition at the surface. The long-term variations of the calculated time-series are in good agreement with the measured variations, especially for the largest considered depth of 40 m. The real effective depth corresponding to the measurement point T1 is difficult to estimate, as the topography of the cliff may play a role; a reasonable value lies between 20 and 40 m. Not only the average increasing trend is well accounted for, but also the comparatively stable temperature period between 2004 and 2014. However, neither the annual amplitude nor its phase can be explained by simple one-dimensional heat diffusion (Fig. 12b). Yet, caution remains necessary. In agreement with the previous observation (Section 7.1), temperature variations in T1 were affected by seepage during the season of positive WE. Thus, the annual heat wave may be modified and might still constitute the main variation, with transients caused by seepage. The groundwater arriving in the deeper parts of the cave is probably not recent rainfall, but old rainfall pushed from above by fresh rainfall, likely by a piston effect (Genty et al., 2004, 2014; Bourdin et al., 2011), hence in thermal equilibrium with the rock above the cave.

Thermal effects due to rainfall are also expected to be more important in the frontal part of the cave, decreasing rapidly when moving inside the cave towards the north (Fig. 1a). The thermal effect of seepage on T0 temperature, the closest to the entrance (collapse structure), depends on the difference between atmospheric temperature and the temperature measured in the debris cone, and thus can be either positive or negative (Fig. 9b). Most of the time, however, the largest seepage events were observed during early fall, when atmospheric temperature becomes smaller than T0 temperature, and the observed temperature change was negative. At this location, in addition, transient infiltration of cold air, during winter, through the porous collapse zone, may also contribute to negative temperature changes. In the case of T1, deeper in the cave, the situation is different (Fig. 9a). At that location, the transit times are longer and the amount of rock material to cross is larger, therefore, seepage water reflects, rather than exterior atmospheric temperature, the mean temperature closer to the ground surface in the rock. As mentioned above (Section 4.1), the Chauvet scarp is characterized by a negative stationary temperature gradient towards the north, and similarly negative from surface to depth. Consequently, away from the entrance zone, if the seepage water temperature is indeed higher than the mean cave temperature at the drip point, then it is reasonable that the effect of water input leads to a temperature increase.

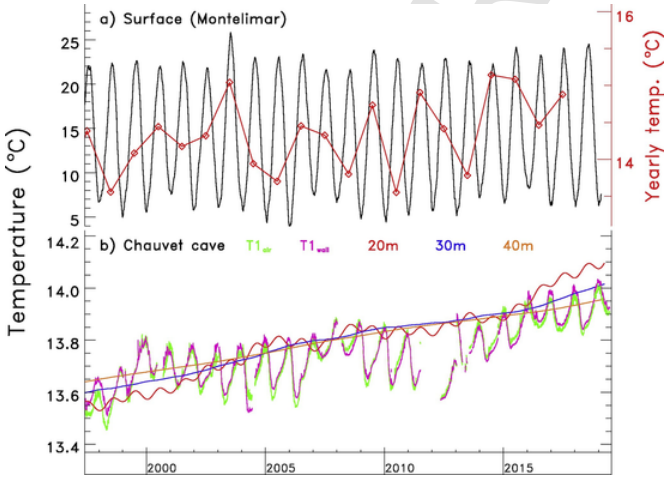

Fig. 12. a) Surface daily temperature at Montélimar averaged with a running window of 48 days (left scale) and yearly mean temperature (right scale). b) Daily temperature in the Brunel Room (T1, scale on the left) with the calculated temperature by heat diffusion from the Montélimar surface temperature at 20 m, 30 m and 40 m depth.

7.2. Seepage as control of CDC: from secondary CDC to primary CO_2 flux

The situation is less straightforward to explain quantitatively with the variations of CDC, but nevertheless physical conceptual models can be proposed. The CO_2 production rate, controlled by temperature and humidity (Jassal et al., 2004; Cook et al., 1998), should be affected by slow seasonal variations. In any case, CO_2 accumulated in the epikarst rocks above the cave is transported down, first in the air phase because of the larger density of air with high CO_2 content. Indeed, assuming a CO_2 content of 8% at the production point, the calculated air density is larger than the density of the cavity air by about 1.2%. In a free volume of 10 m size, the resulting compositional Rayleigh number, which quantifies advection over diffusion, is in excess of 10^{11}, sufficient to cause turbulent double-diffusive convection (Turner, 1973) and flow downward the available topography. This mechanism for example was observed during the dramatic 1986 CO_2 eruption of Lake Nyos, when CO_2 loaded air flowed down a valley and killed >1700 people (Fay, 1988). In a permeable porous medium, the presence of few open cracks would be sufficient to initiate downward motion, with buoyancy still dominating diffusion. Then the CO_2 loaded air flows downwards, while the air with smaller density is displaced upwards. High water vapour content of air has the opposite effect, producing the upward motion of the mixture (Perrier, 2005; Perrier et al., 2002, 2004). This mechanism, which relies on the convective motion of air masses, should not to be confused with sedimentation, which seems to be ruled out in the case of the Chauvet cave and other caves. In addition, such buoyancy-driven transport of air should definitely not be confused with some purely gravitational separation of CO_2 from the air, an effect which has not been evidenced in natural underground systems, dominated by the motion and mixing of underground air (Badino, 2009).

The downward flow could also result in part from groundwater flow, with air volumes travelling down between water volumes in the unsaturated space (Genty et al., 2004; Genty and Deflandre, 1998). However, in the case of the Chauvet cave, groundwater infiltration was dominantly associated with a cessation of the CO_2 flux (e.g., Fig. 9), suggesting that buyancy-driven flow of CO_2-rich air dominates in connected channels, non-saturated by the water phase. Another interesting possibility is that groundwater flowing in the non-saturated zone drags air pockets with a lower CO_2 content, coming from an upper rock or soil layer, while the infiltration that feeds the stationary drippings maintained during the water deficit drain air pockets with a larger CO_2 content, produced over longer residence times in deeper soil.

The difference between the main compartment (A) and the remote room RR (B) also needs to be explained. While the temporal variations are similar (Figs. 2 and 3), a larger CDC by about 1.2% in absolute (60 to 70% in relative, see Table 1), was observed in the RR (CO_2 B,

Fig. 6). At a temperature of 12.9 °C for 100% RH, the specific mass of air in the RR, for a CDC of 3.7%, is about 1250 g/m^3, whereas a specific mass of 1241 g/m^3 is found in the Hillaire Room. Thus, the mean CDC difference between the Hillaire Room and the RR is sufficient in itself to maintain the spatial segregation, in addition to the topographic barrier in the Megaceros Corridor (Supp. Mat. Fig. S7). At such temperature, a 1% (absolute) CDC increase corresponds to a temperature drop of 1.33 °C or a RH decrease of about 100%.

To further clarify the difference between compartments A and B, it is useful to extract the CO_2 source term, namely the CO_2 flux from the walls. Indeed, the measured CDC is only a secondary parameter; it does not only reflect the primary source, which is the flux, but the air motions and atmospheric mixing in the various parts of the cave. To extract the primary flux parameter in compartments A and B, a simplified box model, presented in details in Appendix A, is used to describe the main air exchanges. The resulting flux time-series are in principle model-dependent, and have to be interpreted with caution. However, in this case, the inferred fluxes are rather stable (see Appendix A), especially in the main compartment (Fig. A2).

The time-series of CO_2 fluxes in compartments A and B (Fig. 13a) confirm the control by the hydrological cycle. The flux in compartment A (Fig. 13a) increases regularly during the period of smooth decreasing relaxation of drip counts and water level in the Orgnac borehole (Fig. 13b), associated with periods of water deficit (Fig. 13), highlighted in yellow and defined totally independently from the observations in the cave. In 2016, an exponential growth is clearly observed with a time constant of about two months and a saturation maximum level of 5 g m^{-2} day^{-1}. During periods of high WE, the CO_2 flux in A decreases systematically, but in a fashion that depends on the year, slightly different in 2015 and 2016 (Fig. 13a), probably due to the amount of rainfall and its time pattern. The cumulated CO_2 flux reduction due to seepage seems to have a minimum limit at a constant minimal CO_2 flux of 1.8 g m^{-2} day^{-1}. This value is rather high, much larger than fluxes of the order of 0.1 g m^{-2} day^{-1} inferred for example in the Vincennes quarry (Perrier and Richon, 2010), but compatible with estimates obtained in Orgnac (Bourges et al., 2006).

In the RR (compartment B), the inferred flux, in a first approximation, can be considered constant, given the uncertainties of the mixing model. However, a flux decrease during the water deficit period (highlighted in yellow in Fig. 13) and a flux increase during the positive WE period, are indicated. In this model, the larger CDC in B is explained by a more constant flux throughout the year and a larger confinement. The smaller CDC in A is due in part to the stronger seasonal modulation of the CO_2 flux, and in part to air exchange with the outside atmosphere. It is important to note that air exchange between compartment A and the outside atmosphere, in the box model, is formally equivalent to a sink term. Thus, air exchange, whose signature cannot be confirmed unambiguously by the isotopic data, might actually be smaller than assumed in the box model (Appendix A), but compensated by some loss of CO_2 in the cave, for example from the floor or leaking fractures. In any case, in this model, the similar annual variation in A and B is explained by the air exchange between the two compartments. In the box model, when air exchange between A and B is reduced, the annual amplitude in B decreases, but the mean CDC then reaches values larger than 5%. Thus, the compromise expressed in the choice of parameters in the box model is rather robust, well constrained by the observed features of the data.

Once the features of the primary parameters are established, in this case the CO_2 flux, the mechanisms of temporal variations along the season remain to be understood. Among the possible options, one concep-

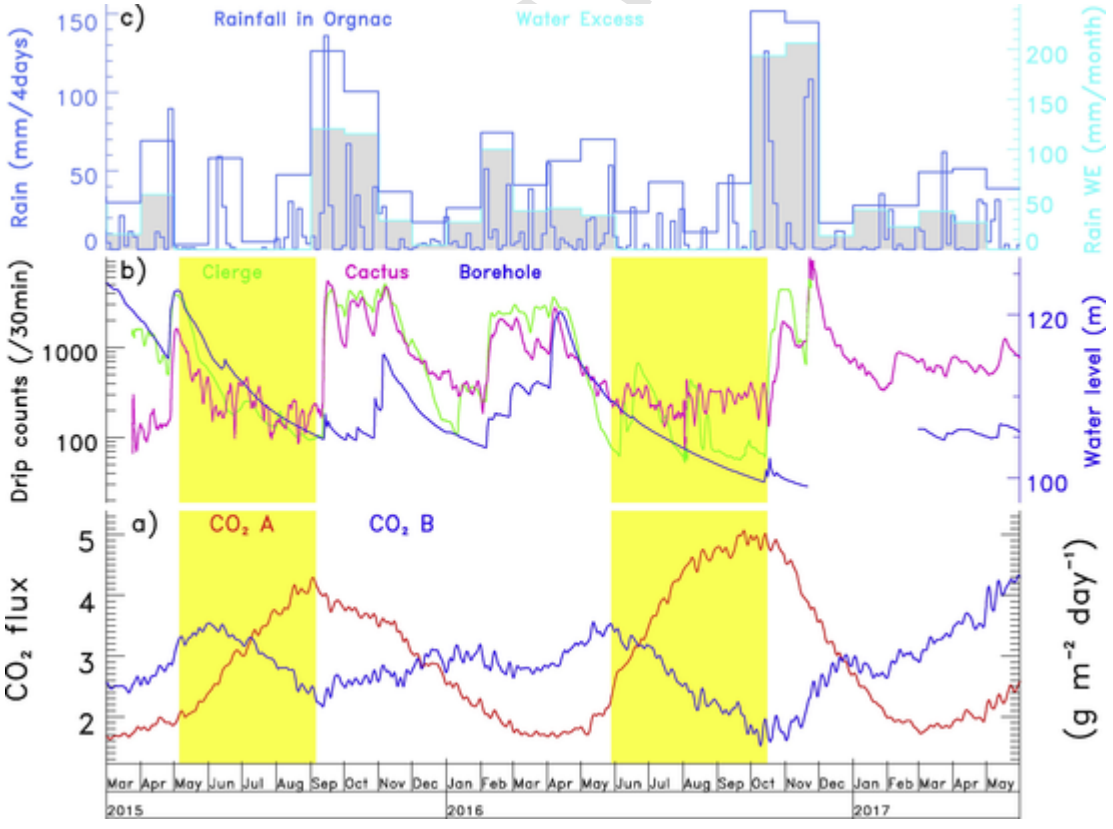

Fig. 13. a) Inferred CO_2 flux into the Chauvet cave. b) Drip counts at Cierge and at Cactus (left scale) and daily water level in the Orgnac borehole (right scale). The drip counts are filtered with a running window of 12 h. c) Rainfall per 4 days at Orgnac (left scale) with monthly rainfall and calculated Water Excess (right scale). Periods with no Water Excess and restoration of CO_2 in the main room A are highlighted with yellow background. (For interpretation of the references to colour in this figure legend, the reader is referred to the web version of this article.)

tual model for CO_2 transport from the CO_2 production zone can be proposed.

7.3. Scenario with horizontal and vertical transport of CO_2

A tentative conceptual model for CO_2 transport at scarp level can be proposed (Fig. 14). In this case, CO_2 enters the cave through horizontal dispersed flow, rather than vertical flow through localized channels. In this framework, both SC and GC flow downwards by buoyancy entrainment, but are accumulated in connected porosity to form a structure similar to a free aquifer (Fig. 14). Vertical CO_2 flow from the sources is then similar to infiltration. Porosity is probably not homogeneous in the epikarst, which in this case has a thickness of 5 to 10 m, and in the whole vadose zone above the aquifer level, which, in the case of the Chauvet cave, is below the cavity floor, probably just above the abandoned river meander (Supp. Mat. Fig. S1). Instead, CO_2 probably flows through highly connected, dense cracks. The CO_2 accumulated in these non-saturated reservoirs, will undergo horizontal flow similar to the horizontal mean flow in a free aquifer (Fig. 14), and then feeds into the cavity from the side and, possibly, from the roof as well. Several reservoirs can communicate with each other and flow into each other like water reservoirs (Fig. 14). The CO_2 of RR primarily originates from the bedrock, rather than from the Hillaire Room through the Megaceros Corridor. It could in fact completely fill the remaining of the cave from the RR, but the topography of the Megaceros Corridor is an efficient barrier. When rainfall occurs, the porosity controlling the CO_2 flow is invaded by water and the input CO_2 flow into the cave is dramatically reduced or even stopped.

The analogy between this horizontal CO_2 model and a free aquifer can be pushed further by proposing an analogy with the Dupuit approximation of aquifer theory (Bear, 1988). In this approximation, the CO_2 flow rate F is considered to be horizontal and uniform vertically over the whole CO_2 reservoir, and can be given by:

$$\vec{F} = -K\vec{\nabla}h_{CO_2}, \quad (1)$$

where K is the hydraulic conductivity of the porous formation and h_{CO2} would be an equivalent CO_2 piezometric level, given by the integral of the vertical column of the air density. All concepts of aquifer theory can then be transferred to CO_2 flow. The equivalent of the aquifer piezometric surface could be the level where the bedrock CDC is a reference value, typically 5 to 7%, depending on the context. In this framework, temporal variations of the input flow into the cavity should be slow, damped by the porous medium diffusivity, similar to the stability of a spring flow rate versus rainfall. This model of CO_2 reservoir flow may thus account for the largest part of the seasonal variation. The long-term variations remain more difficult to explain in a systematic manner, with the long-term role of seepage not sufficiently clear (Fig. 10), but the increase of vegetation density, revealed by the aerial photographs (1955–2012) may explain the long inter-annual increasing CO_2 trend (Supp. Mat. Fig. S1).

8. Conclusions and perspectives

8.1. Observations and importance of water infiltration

We have presented in this study the main features of carbon dioxide concentration (CDC) observed in the Chauvet-Pont d'Arc painted cave, where large natural ventilation can be ruled out. While temperatures were relatively stable, CDC exhibits large seasonal and transient variations, a global increasing trend since the beginning of the measurement (1997), and a spectacular increasing trend from 2013 to 2017, followed by a decrease. Seasonal CDC variations in underground settings have been observed since decades (Troester and White, 1984), but such large seasonal variations in deep caves in the absence of seasonal natural ventilation cycles had not been observed before. The main factor controlling the seasonal CO_2 input into the cavity and its isotopic signature is water infiltration following rainfall. The regular increase of mean CDC can then be attributed to the decrease of precipitation from April to September observed between 2013 and 2017, and interrupted by heavy rainfall at the end of 2017 and in 2018. Such pluri-annual effects or long-term trends, however, have not been observed systematically since 1997. Long-term changes of CDC might be due to changes in the CO_2 production associated with the evolution of vegetation cover over the cave, possibly combined with changes in the outside temperature, rather than with changes in CO_2 transport through seepages only. No relationship has been observed between CDC in the cave and biological germs in the air cave, which remained at low concentrations; therefore an evolution of the biological activity in the cave itself is ruled out. Another important conclusion of this work is that water infil-

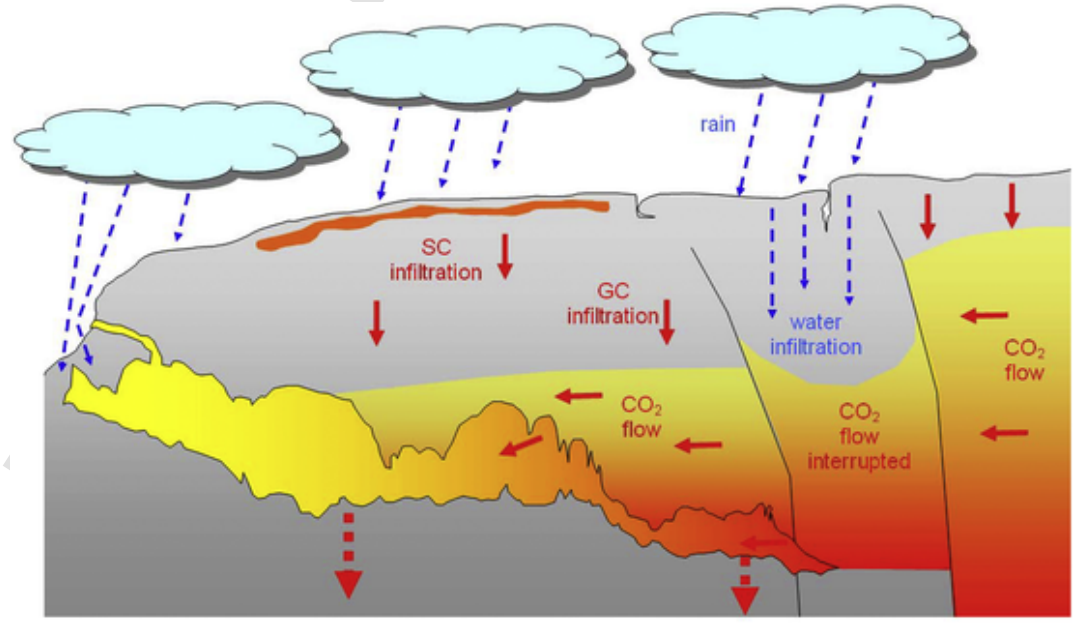

Fig. 14. Conceptual model of CO_2 input into the Chauvet cave atmosphere (CO_2 reservoir flow model).

tration also modulates the seasonality of the temperatures inside the cave, while the global increasing trend of temperatures is accounted for by heat diffusion from the surface.

To evidence the importance of the effect of seepages on CDC, three important tools have unambiguously proven their usefulness. The first essential asset is given by drip count data, associated with the calculation of the meteorological water balance, which can be listed as the second important tool. Seasonal regimes of CDC variations, indeed, appeared efficiently predicted by the calculation of WE (Genty, 2008; Genty and Quinif, 1996). Thirdly, to interpret the physical conditions in a cave, it is important to extract primary parameters that provide information on the sources, from the secondary observed parameters, such as CDC, affected not only by sources but also by internal air exchanges or further complications.

While the seasonal hydrological cycle is considered as the main causal factor causing the seasonality of the CDC in the cave, the effect of seasonal temperature changes should not be underestimated. First, the seasonal outside temperature cycle, explicitly included in the calculation of WE, plays an important role in the infiltration. Given the southward exposure, temperature must also strongly affect the CO_2 production in the debris cone obstructing the natural entrance of the cave. However, the total surface area from that particular zone is small compared with the total volume of the Chauvet cave.

From its isotopic signature, the source of CO_2 must be located in the soil and below, with older carbon feeding the deeper parts of the cave. Two distinct GC sources by $\delta^{13}C$ values are suggested, but this must be confirmed by a more detailed study. Transport mechanisms of CO_2 into the cave remain to be clarified further, but a horizontal CO_2 reservoir flow model at the cliff scale, driven by the buoyancy deficit due to the CO_2 content, appears promising, as it is able to describe, at least qualitatively, the effect of water seepage. This model is testable and can be considered as the baseline for future work. As the main regimes of temporal variations of drip counts appeared homogeneous and almost synchronous inside the cave, and even similar to water level variations in a borehole located in Orgnac, 7 km from the cave, the relationship between cave CDC and transient seepage can be studied at other underground sites with similar geometry and depth below ground surface. Alternatively, the CO_2 sources could also be at depth, below the cave floor, but, in this context, the temporal variability would be more difficult to explain, and this option is not considered at this stage.

8.2. Cave climate, preservation and climate changes

Several consequences of our observations and interpretations can be proposed. First, in a past colder and more humid climate, with a wet vadose zone under melting snow and ice layers, and an associated reduced production of CO_2 in the soil, we expect that CDC in the Chauvet cave was smaller. This should be true in other caves, with earlier Homo Sapiens and even Neanderthal occupation (Hoffmann et al., 2018; Jaubert et al., 2016). The current values of CDC are incompatible with long periods of presence in a confined cave. It has been suggested that, at the time of human occupation of the Chauvet cave, the entrance of the cave was wide open (Sadier et al., 2012), without the debris cone, allowing for efficient natural ventilation. The second consequence is that, if the water content in the vadose zone above the Chauvet cave decreases, with more variability and more frequent periods with a decrease of summer precipitation, and an increase of water deficit due to the temperature increase, then even larger CDC peak values can be expected. When the CDC in the cave will be larger than 5%, human presence during maintenance or archaeological work will not be possible without breathing accessories and oxygen supply, since artificial ventilation is not here an acceptable option. Thus, the period of CDC increase from 2013 to 2017, first of all, is symptomatic of an overall fragile situation, possibly diverging when climate will affect dramatically the soil vegetation cover, a situation which puts the cave and its precious paintings at risk.

Climate change in the region of the Chauvet cave is a reality, and is expected to lead to dramatic consequences, including drought, in the whole region around the Mediterranean sea (Allard et al., 2008). Possible reductions of the effects due to the overall drought, resulting from counter-reaction from root respiration (Rodriguez-Calcerrada et al., 2014), are unlikely to play an important role in the calcareous soil biotope above the Chauvet cave. The expected effects resulting from water deficit in the vadose zone are more of a concern than the possible slow increase of the mean underground temperature (Perrier et al., 2005a). In general, the damaging effects of climate change to the subsurface and to the lower part of the CZ have probably been largely underestimated till now.

The current trend observed in the Chauvet cave, however, is not confirmed in caves in South-West France (Table 1). It is therefore premature to draw drastic conclusions at this stage, and the proposed model and interpretation need to be studied in details. It is also possible that the effects revealed in the Chauvet cave are also present in the caves of South-West France, yet concealed by natural ventilation or human intervention. A cave with a geometry and situation similar to the Chauvet cave would be needed in the South-West region to provide a relevant reference; this seems difficult and no candidate site is available at the moment. The dynamics of CO_2 inside the cave also needs to be better understood, and, to address the non-stationary behaviour, heuristic concepts could be of value (Sánchez-Cañete et al., 2013; Denis et al., 2005). In addition to CDC data, radon concentration (Perrier and Richon, 2010) and aerosol data (Dredge et al., 2013) are important additional parameters to monitor to be able to constrain the processes in the Chauvet cave atmosphere. Detailed radon data would allow, in particular, constraining the air exchange rates independently of the CO_2 data. Particle counting would also bridge the gap between physical parameters of the cave atmosphere and its biological activity, which is essential to carefully monitor for preservation.

Beyond global effects, the consequences of CDC changes in the Chauvet cave need to be worked out. While CDC plays an important role in speleothem growth and the painting preservation (Bourdin et al., 2011), other factors, such as relative humidity, chemical composition of dripping water and biophysical conditions of the painting surfaces (Vouvé et al., 2000; Sanchez-Moral et al., 1999), might be of greater importance. At this stage, it is too early to draw any conclusion on the preservation of the paintings in the presence of larger or more unstable CDC. It is also not excluded that, in the long-term, the cavity might also develop adaptive and even resilient mechanisms to the current environmental changes. Counter-reaction mechanisms through phase changes of water (Perrier et al., 2002, 2004) are remarkably efficient to guaranty thermal stability. Biological adaptation and feedbacks to increased SG and GC CDC are also possible in principle.

Some features of the Chauvet cave, by themselves, could provide efficient protective factors. The high levels of CO_2 may play an important role in stabilizing the atmosphere against small temperature changes, separately in the different compartments with stable interfaces, and possibly against larger effects due to climate changes such as infiltration regimes. The smooth variations of CDC, contrasting with the drastic changes observed in caves undergoing dynamic ventilation, may also play an important role in stabilizing the chemical reactions at the wall surfaces, including the paintings. The stability of the vertical temperature gradients, with colder temperatures in the deeper parts, and warmer temperature near the roofs and towards the front of the cliff, also offers an important protective factor for the remains.

On the other hand, the increase of variability near the entrance may be a concern in the long term, and divergent reactions of natural sites in the presence of unusual perturbations are possible. Dramatic and spectacular reactions of natural deep systems in the presence of CO_2 in-

jection, rather than adaptation, have now been documented (Trias et al., 2017). Therefore, it is clearly an important recommendation to survey and evaluate long-term approaches for the vegetation cover above painted caves, and to implement an associated detailed monitoring of the soil properties. Since 1980, the strategy in the natural reserve above the Chauvet cave was to guaranty a natural development of the vegetation, but this may cause an increase of the carbon mass potentially degraded in the soil and subsurface, which ultimately may cause a novel situation in the cave. The associated processes are not sufficiently known at this time and require an improved understanding. To clarify the sources and transport mechanisms of CDC in underground environments, especially in the case of painted caves, joint experimental and theoretical efforts will need to be dedicated with increasing attention in the coming decades.

Declaration of competing interest

The authors declare no conflict of interest.

Acknowledgements

Monitoring and isotopic analyses have been partly funded by INSU/CNRS research program CALSPEL (2014-2016; coordinator DG). The French Ministry of Culture (Heritage), Dominique Baffier, Marie Bardisa and the scientific team of the Chauvet cave are thanked for allowing the cave visits and for supporting the climatologic and hydrologic studies. Michel Lorblanchet is thanked for numerous discussions and advice on all aspects of the conservation of painted caves. The original manuscript was considerably improved thanks to the careful work of two anonymous reviewers. This paper is IPGP contribution number xxxx.

Appendix A. Box modelling and determination of the carbon dioxide flux into the Chauvet cave

The CDC measured in the underground atmosphere results from CO_2 sources located in the cavity, CO_2 flux from the cavity walls, and air exchange. Internal sources, such as microbiological activity in the cave or degassing from the infiltrating water and its interaction with speleothem, can be considered as negligible compared with the intense CO_2 production taking place above the cavity. In a first approximation, it is legitimate to assume that the main CO_2 input factor into an underground cavity is equivalent to some surface flux at the cavity boundaries, dominated in this case by the roof surface, with some contribution from the side walls. To describe the spatial and temporal evolution of CDC, a Computational Fluid Dynamics (CFD) approach can be used (Lacanette et al., 2009), but, given the large number of unknowns, a simplified box modelling approach appears relevant (Perrier et al., 2005b). The underground system is then represented by a small number of well mixed boxes, with air exchanges between the various boxes and with the outside atmosphere.

In the case of the Chauvet cave, the observations suggest that CDC is uniform in the two compartments A and B, with no evidence for vertical stratification (Fig. 5). We thus model the cavity (Fig. A1) by two well mixed boxes A and B, which are each characterized by their volumes V_A and V_B, surface areas S_A and S_B, and their CO_2 surface fluxes F_A and F_B, respectively. Air exchange takes place with the outside atmosphere, characterized by CDC C_e, with a volumetric rate a, and between the compartments A and B with an air exchange rate b. The time evolution of the resulting CDC, C_A and C_B in the two compartments, is then given by:

$$\begin{cases} \frac{dC_A}{dt} = \frac{S_A F_A}{V_A} - a\left(C_A - C_e\right) - b\left(C_A - C_B\right) \\ \frac{dC_B}{dt} = \frac{S_B F_B}{V_B} + b\frac{V_A}{V_B}\left(C_A - C_B\right) \end{cases}, \tag{A1}$$

where the ratio V_A/V_B in the second equation guarantees mass conservation between compartments A and B, and that the total content $V_A C_A + V_B C_B$ does not depend on b.

From the observed CDC, the system (A1) can also be rewritten to extract the fluxes:

$$\begin{cases} F_A(t) = \frac{V_A}{S_A}\left[\frac{dC_A}{dt} + a\left(C_A - C_e\right) + b\left(C_A - C_B\right)\right] \\ F_B(t) = \frac{V_B}{S_B}\left[\frac{dC_B}{dt} - b\frac{V_A}{V_B}\left(C_A - C_B\right)\right] \end{cases}. \tag{A2}$$

These inferred fluxes are model-dependent, as an assumption on the ventilation rates and their time dependence is necessary to be able to apply Eq. (A2). In practice, the time derivatives of the concentrations can be difficult to estimate at each sampling time. Here, we used an estimate of the derivative defined as the slope, at sample i, provided by a linear fit from samples i to $i + k$, with $k = 384$ (4 days). The obtained fluxes are then reasonably smooth (Fig. A2). In the following, we use $V_A = 28{,}000\ m^3$ and $V_B = 2000\ m^3$, $S_A/V_A = S_B/V_B = 1.5$, and mean exchange rates $a = 1.5 \times 10^{-6}\ s^{-1}$ and $b = 1.5 \times 10^{-7}\ s^{-1}$, which are reasonable values expected for poorly ventilated sites (Perrier and Richon, 2010; Perrier et al., 2007; Richon et al., 2005).

In the default case (case 1 in Fig. A2), we assumed that the exchange rates are modulated by an annual variation of peak-to-peak amplitude $4 \times 10^{-7}\ s^{-1}$ and $7.5 \times 10^{-8}\ s^{-1}$ for a and b, respectively (green curve for $a(t)$ and purple curve for $b(t)$ in Fig. A2b). The presence of an annual variation of the ventilation rate is not clearly confirmed in the Chauvet cave with the current data, but is a common feature in such systems (Bourges et al., 2001). The available radon-222 time-series (Fig. 5) indicated a rather stable concentration, with a maximum seasonal variation of the order of 10%. The assumed values of the annual variation of the ventilation rates are therefore upper limits. When the annual variations of the ventilation rates are removed (case 2 in Fig. A2c), the inferred fluxes are not dramatically different. When a larger value of $2 \times 10^{-7}\ s^{-1}$ is used for b (case 3 in Fig. A2b), more significant differences are observed for flux F_B, while F_A remains essentially the same (Fig. A2c). Consequently, given the large uncertainty on the exchange rate b, caution is mandatory when interpreting the obtained flux F_B in the RR, while the mean flux in the main rooms, F_A, can be considered rather reliable.

The box model can also be used to derive general properties. In the stationary state, characterized by static concentrations $\overline{C}_A$ and $\overline{C}_B$, we have:

$$\begin{cases} \overline{C}_A = \overline{C}_e + \frac{S_A \bar{F}_A + S_B \bar{F}_B}{\bar{a} V_A} \\ \overline{C}_B = \overline{C}_A + \frac{S_B \bar{F}_B}{\bar{b} V_A} \end{cases}, \tag{A3}$$

where $\bar{F}_A$, $\bar{F}_B$, $\bar{a}$ and $\bar{b}$ are the mean values of the CO_2 fluxes and exchange rates.

Time constants can be derived when the exchange rates are independent of time. The concentrations are then written as perturbations of the stationary state:

$$\begin{cases} C_A(t) = \overline{C}_A + c_A(t) \\ C_B(t) = \overline{C}_B + c_B(t) \end{cases}, \tag{A4}$$

and the time evolution can be written as:

$$\frac{d}{dt}\begin{pmatrix} c_A \\ c_B \end{pmatrix} = M\begin{pmatrix} c_A \\ c_B \end{pmatrix}, \tag{A5}$$

with:

$$M = \begin{bmatrix} -(a+b) & b \\ b\frac{V_A}{V_B} & -b\frac{V_A}{V_B} \end{bmatrix}. \tag{A6}$$

The matrix M has two negative eigenvalues $\lambda_{\pm} = -1/\tau_{\pm}$, where $\tau_{\pm}$ are two time constants, with $\tau_+ < \tau_-$, given by:

$$\tau_{\pm} = \frac{2}{a + b\left(1 + \frac{V_A}{V_B}\right) \pm \sqrt{\left[a + b\left(1 + \frac{V_A}{V_B}\right)\right]^2 - 4ab\frac{V_A}{V_B}}}. \tag{A7}$$

When V_A is much larger than V_B, which is the case considered here, the time constants are given by:

$$\tau_+ = \frac{1}{a} \text{ and } \tau_- = \frac{V_B}{bV_A}. \tag{A8}$$

For the values of the parameters considered above, we have $\tau_+ \cong 4.7$ days and $\tau_- \cong 9.1$ days. Such timescales are probably intrinsic properties of the site, which will probably be preserved in more detailed CFD models.

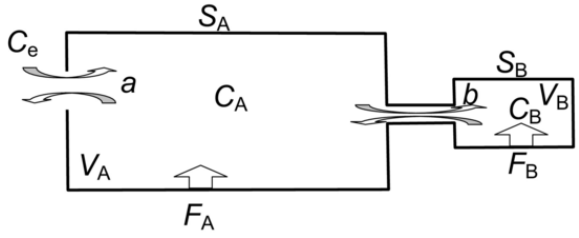

Fig. A1. Sketch of the box model (see text for the definition of parameters).

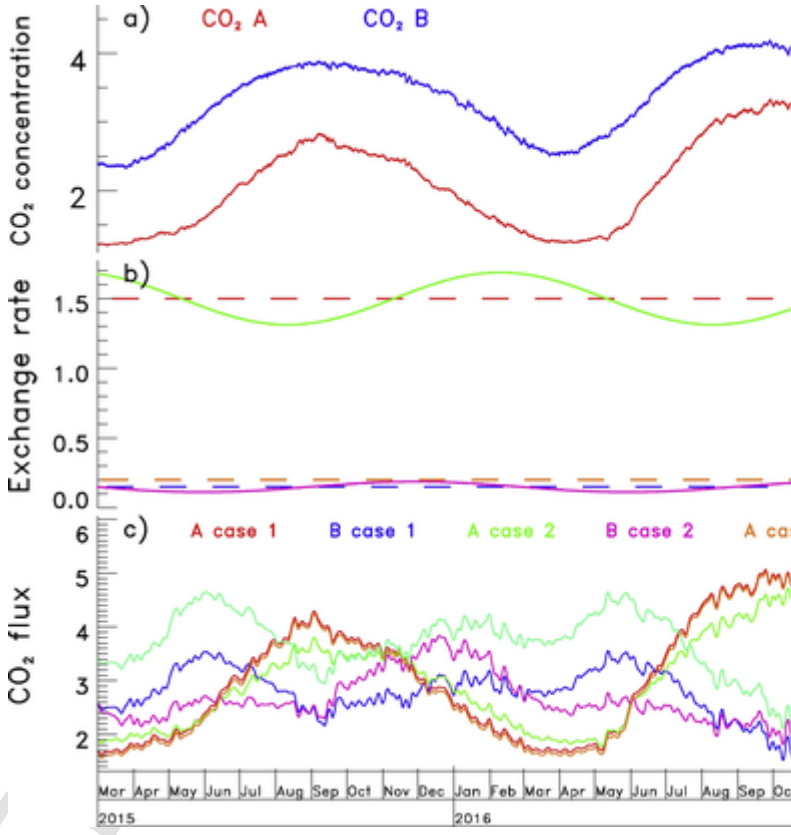

Fig. A2. Calculated CO_2 flux: a) Measured CDC versus time in the Chauvet cave; b) assumed exchange rates a and b versus time (the red dashed line indicates the mean value for a, the blue dashed line represents the mean value for b and the orange dashed line is the mean value for b in case 3); c) Inferred CO_2 fluxes in A and B compartments versus time. (For interpretation of the references to colour in this figure legend, the reader is referred to the web version of this article.)

Appendix B. Supplementary data

Supplementary data to this article can be found online at https://doi.org/10.1016/j.scitotenv.2020.136844.

References

Allard, V., Ourcival, J.-M., Rambal, S., Joffre, R., Rocheteau, A., 2008. Seasonal and annual variation of carbon exchange in an evergreen Mediterranean forest in southern France. Glob. Chang. Biol. 14, 714–725.

Atkinson, T.C., 1977. Carbon dioxide in the atmosphere of the unsaturated zone: an important control of groundwater hardness in limestones. J. Hydrol. 35, 111–123.

Badino, G., 2004. Cave temperatures and global climatic change. Int. J. Speleol. 33, 103–114.

Badino, G., 2009. The legend of carbon dioxide heaviness. J. Cave Karst Stu. 71 (100–107), 2009.

Baker, A., Genty, D., 1998. Environmental pressures on conserving cave speleothems: effects of changing surface land use and increased cave tourism. J. Environ. Manag. 53, 165–175.

Balakowicz, M., Jusserand, C., 1986. Étude de l'infiltration en milieu karstique par les méthodes géochimiques et isotopiques: cas de la grotte de Niaux (Ariège, France). Bull. Centre Hydrogéol Neuchâtel 7, 265–283. (In French).

Batiot-Guilhe, C., Seidel, J.-L., Jourde, H., Hébrard, O., Bailly-Comte, V., 2007. Seasonal variations of CO_2 and ^{222}Rn in a mediterranean sinkhole-spring (Causse d'Aumelas, SE France). Int. J. Speleol. 36, 51–56.

Bear, J., 1988. Dynamics of Fluids in Porous Media. Dover Publications, New York. (764 pp).

Beltrami, H., Ferguson, G., Harris, R.N., 2005. Long-term tracking of climate change by underground temperatures. Geophys. Res. Lett. 32, L19707.

Benavente, J., Vadillo, I., Carrasco, F., Soler, A., Liñán, C., Moral, F., 2010. Air carbon dioxide contents in the vadose zone of a Mediterranean karst. Vadose Zone 9, 126–136.

Bourdin, C., Douville, E., Genty, D., 2011. Alkaline-earth metal and rare-earth element incorporation control by ionic radius and growth rate of a stalagmite from the Chauvet cave, Southeastern France. Chem. Geol. 290, 1–11.

Bourges, F., Mangin, A., D'Hulst, D., 2001. Carbon dioxide in karst cavity atmosphere dynamics: the example of the Aven d'Orgnac (Ardèche). C. R. Acad. Sci. Paris 333, 685–692.

Bourges, F., Genthon, P., Mangin, A., D'Hulst, D., 2006. Microclimate of l'Aven d'Orgnac and other French limestone caves (Chauvet, Esparros, Marsoulas). Int. J. Climatol. 26, 1651–1670.

Bourges, F., Genthon, P., Genty, D., Mangin, A., D'Hulst, D., 2012. Comment on "Carbon uptake by karsts in the Houzhai Basin, southwest China" by Junhua Yan et al. J. Geophys. Res. 117, G03006.

Bourges, F., Genthon, P., Genty, D., Lorblanchet, M., Mauduit, E., D'Hulst, D., 2014. Conservation of prehistoric caves and stability of their inner climate: lessons from Chauvet and other French caves. Sci. Tot. Environ. 493, 79–91.

Bourges, F., Mangin, A., Genthon, P., Genty, D., D'Hulst, D., Mauduit, E., 2014. Conservation and handling of decorated prehistoric caves: lessons from environmental monitoring at Chauvet-Pont d'Arc cave. Paleo Special Issue 339–345.

Brodovsky, D., Macdonell, J.A., Cherniak, R.M., 1960. The respiratory response to carbon dioxide in health and in emphysema. J. Clin. Inv. 39, 724–729.

Chiodini, G., Caliro, S., Cardellini, C., Avino, R., Granieri, D., Schmidt, A., 2008. Carbon isotopic composition of soil CO_2 efflux, a powerful method to discriminate different sources feeding soil CO_2 degassing in volcanic-hydrothermal areas. Earth Planet. Sci. Lett. 274, 372–379.

Choppy, J., 1965. La sédimentation du gaz carbonique. Ann. Spéléol. 20, 449–451. (In French).

Clottes, J., Chauvet, J.-M., Brunel-Deschamps, E., Hillaire, C., Daugas, J.-P., Arnold, M., Cachier, H., Evin, J., Fortin, P., Oberlin, C., Tisnérat, N., Valladas, H., 1995. Les peintures paléolithiques de la grotte Chauvet-Pont d'Arc, à Vallon-Pont d'Arc (Ardèche, France): datations directes et indirectes par la méthode du radiocarbone. C. R. Acad. Sci. Paris IIA, 1133–1140. (In French).

Clottes, J., Arnold, M., Aujoulat, N., Baffier, D., Debard, É., Delannoy, J.-J., Évin, J., Feruglio, V., Fosse, P., Ferrier, C., Fritz, C., Garcia, M.-A., Gély, B., Geneste, J.-M., Girard, M., Guérin, C., Kervazo, B., Le Guillou, Y., Maksud, F., Morel, P., Oberlin, C., Parker, C., Perrette, Y., Philippe, M., Robert-Lamblin, J., Rouzaud, F., Schefer, J.-L., Tisnérat, N., Tosello, G., Valladas, H., 2001. La Grotte Chauvet: L'Art des origines, Seuil, Paris. (226 pp. In French).

Conn, H.W., 1966. Barometric wind in Wind and Jewel Caves, South Dakota. Bull. Nat. Speleol. Soc. 28, 55–69.

Cook, F.J., Thomas, S.M., Kelliher, F.M., Whitehead, D., 1998. A model of one-dimensional steady-state carbon dioxide diffusion from soil. Ecol. Model. 109, 155–164.

Crouzeix, C., Le Mouël, J.-L., Perrier, F., Richon, P., 2006. Thermal stratification induced by heating in a non-adiabatic context. Build. Environ. 41, 926–939.

Cuezva, S., Fernandez-Cortes, A., Benavente, D., Serrano-Ortiz, P., Kowalski, A.S., Sanchez-Moral, S., 2011. Short-term CO_2 (g) exchange between a shallow karstic cavity and the external atmosphere during summer: role of the surface soil layer. Atmos. Environ. 45, 1418–1427.

De Freitas, C.R., Littlejohn, R.N., 1987. Cave climate: assessment of heat and moisture exchange. J. Climat. 7, 553–569.

De Freitas, C.R., Littlejohn, R.N., Clarkson, T.S., Kristament, I.S., 1982. Cave climate: assessment of airflow and ventilation. J. Climat. 2, 383–397.

Denis, A., Lastennet, R., Huneau, F., Malaurent, P., 2005. Identification of functional relationships between atmospheric pressure and CO_2 in the cave of Lascaux using the concept of entropy of curves. Geophys. Res. Lett. 32, L05810.

Dlugokencky, E.J., Hall, B.D., Montzka, S.A., Dutton, G., Mühle, J., Elkins, J.W., 2018. Atmospheric composition. In: State of the Climate in 2017. In: Bull. Am. Meteo. Soc, 99. pp. S46–S49.

Dominguez-Villar, D., Lojen, S., Krklec, K., Baker, A., Fairchild, I.J., 2014. Is global warming affecting cave temperatures? Experimental and model data from a paradigmatic case study. Clim. Dyn. 2014. doi:10.1007/s00382-014-2226-1.

Dörr, H., Münnich, K.O., 1986. Annual variations of the ^{14}C content of soil CO_2. Radiocarbon 28, 338–345.

Dredge, J., Fairchild, I.J., Harrison, R.M., Fernandez-Cortes, A., Sanchez-Moral, S., Jurado, V., Gunn, J., Smith, A., Spötl, C., Mattey, D., Wynn, P.M., Grassineau, N., 2013. Cave aerosols: distribution and contribution to speleothem geochemistry. Quat. Sci. Rev. 63, 23–41.

Dumoulin, J.-P., Comby-Zerbino, C., Delqué-Količ, E., Moreau, C., Caffy, I., Hain, S., Perron, M., Thellier, B., Setti, V., Berthier, B., Beck, L., 2017. Status report on sample preparation protocols developed at the LMC14 Laboratory, Saclay, France: from sample collection to 14C AMS measurement. Radiocarbon 59, 713–726.

Ek, C., Gewelt, M., 1985. Carbon dioxide in cave atmospheres. New results in Belgium and comparison with some other countries. Earth Surf. Proc. Landforms 10, 173–187.

Faimon, J., Ličbinská, M., Zajíček, P., 2012. Relationship between carbon dioxide in Balcarka Cave and adjacent soils in the Moravian Karst region of the Czech Republic. Int. J. Speleol. 41, 17–28.

Fay, J.A., 1988. Modeling the Lake Nyos gas disaster. Atmos. Environ. 22, 417–418.

Fernandez-Cortes, A., Sanchez-Moral, S., Cuezva, S., Cañaveras, J.C., Abella, R., 2009. Annual and transient signatures of gas exchange and transport in the Castañar de Ibor cave (Spain). Int. J. Speleol. 38, 153–162.

Fernandez-Cortes, A., Cuezva, S., Sanchez-Moral, S., Cañaveras, J.C., Porca, E., Jurado, V., Martin-Sanchez, P.M., Saiz-Jimenez, C., 2011. Detection of human-induced environmental disturbances in a show cave. Environ. Sci. Pollut. Res. 18, 1037–1045.

Fleyfel, M., 1979. Étude hydrologique, géochimique et isotopique des modalités de minéralisation et de transfert du carbone dans la zone d'infiltration d'un aquifère karstique: le Baget (Pyrénées ariégeoises) Thesis Doct. Ingénieur Univ. P. et M. Curie. (221 pp. In French).

Genty, D., 2008. Palaeoclimate research in Villars cave (Dordogne, SW-France). Int. J. Speleol. 37, 173–191.

Genty, D., 2012. Les spéléothèmes de la grotte Chauvet-Pont d'Arc apports chronologiques et paléoclimatiques - Synthèse des travaux publiés. In: Karsts - Paysages et Préhistoire, 13. Collection EDYTEM, pp. 79–88. (In French).

Genty, D., Deflandre, G., 1998. Drip flow variations under a stalactite of the Père Noël cave (Belgium). Evidence of seasonal variations and air pressure constraints. J. Hydrol. 211, 208–232.

Genty, D., Massault, M., 1997. Bomb ^{14}C recorded in laminated speleothems - part 1: dead carbon proportion calculation. Radiocarbon 39, 33–48.

Genty, D., Massault, M., 1999. Carbon transfer dynamics from bomb-^{14}C and $\delta^{13}C$ time series of a laminated stalagmite from SW France – Modelling and comparison with other stalagmite records. Geochim. Cosmochim. Acta 63, 1537–1548.

Genty, D., Quinif, Y., 1996. Annually laminated sequences in the internal structure of some Belgian stalagmites-importance for paleoclimatology. J. Sed. Res. 66, 275–288.

Genty, D., Vokal, B., Obelic, B., Massault, M., 1998. Bomb ^{14}C time history recorded in two modern stalagmites - importance for soil organic matter dynamics and bomb ^{14}C distribution over continents. Earth Planet. Sci. Lett. 160, 795–809.

Genty, D., Ghaleb, B., Plagnes, V., Causse, C., Valladas, H., Blamart, D., Massault, M., Geneste, J.-M., Clottes, J., 2004. TIMS U/Th and 14C AMS ages of the Chauvet cave stalagmites: interest for the chronology of natural and human events of the cave. C. R. Palevol 3, 629–642.

Genty, D., Blamart, D., Ghaleb, B., 2005. Apport des stalagmites pour l'étude de la grotte Chauvet: datations absolues U/Th (TIMS) et reconstitution paléoclimatique par les isotopes stables de la calcite. Bull. Soc. Préhist. Fr. 202, 1–18. (In French).

Genty, D., Labuhn, I., Hoffmann, G., Danis, P.A., Mestre, O., Bourges, F., Wainer, K., Massault, M., Van Exter, S., Régnier, E., Orengo, P., Falourd, S., Minster, B., 2014. Rainfall and cave water isotopic relationships in two South-France sites. Geochim. Cosmochim. Acta 131, 323–343.

Girault, F., Bollinger, L., Bhattarai, M., Koirala, B.P., France-Lanord, C., Rajaure, S., Gaillardet, J., Fort, M., Sapkota, S.N., Perrier, F., 2014. Large-scale organization of carbon dioxide discharge in the Nepal Himalayas. Geophys. Res. Lett. 41, 6358–6366.

Girault, F., Adhikari, L.B., France-Lanord, C., Agrinier, P., Koirala, B.P., Bhattarai, M., Mahat, S.S., Groppo, C., Rolfo, F., Bollinger, L., Perrier, F., 2018. Persistent CO_2 emissions and hydrothermal unrest following the 2015 earthquake in Nepal. Nat. Commun. 9, 2956.

Graven, H., Allison, C.E., Etheridge, D.M., Hammer, S., Keeling, R.F., Levin, I., Meijer, H.A.J., Rubino, M., Tans, P.P., Trudinger, C.M., Vaughn, B.H., White, J.W.C., 2017. Compiled records of carbon isotopes in atmospheric CO_2 for historical simulations in CMIP6. Geosci. Mod. Dev. 10, 4405–4417.

Groppo, C., Rolfo, F., Castelli, D., Mosca, P., 2017. Metamorphic CO_2 production in collisional orogens: Petrological constraints from phase diagram modeling of Himalayan, scapolite bearing, calc-silicate rocks in the NKC(F)MAS(T)-HC system. J. Petrol. 58, 53–83.

Hoffmann, D.L., Standish, C.D., García-Diez, M., Pettitt, P.B., Milton, J.A., Zilhão, J., Alcolea-González, J.J., Cantalejo-Duarte, P., Collao, H., de Balbín, R., Lorblanchet, M., Ramos-Muñoz, J., Weniger, G.-C., Pike, A.W.G., 2018. U-Th dating of carbonate crusts reveals Neandertal origin of Iberian cave art. Science 359, 912–915.

Houillon, N., Lastennet, R., Denis, A., Malaurent, P., Minvielle, S., Peyraube, N., 2017. Assessing cave internal aerology in understanding carbon dioxide (CO_2) dynamics: implications on calcite mass variation on the wall of Lascaux cave (France). Environ. Earth Sci. 76, 170.

Hoyos, M., Soler, V., Cañaveras, J.C., Sanchez-Moral, S., Sanz-Rubio, E., 1998. Microclimatic characterization of a karstic cave: human impact on microenvironmental parameters of a prehistoric rock art cave (Candamo cave, northern Spain). Environ. Geol. 33, 231–242.

Jassal, R.S., Black, T.A., Drewitt, G.B., Novak, M.D., Gaumont-Guay, D., Nesic, Z., 2004. A model of the production and transport of CO_2 in the soil: predicting soil CO_2 concentrations and CO_2 efflux from a forest floor. Agr. Forest Meteo. 124, 219–236.

Jaubert, J., Verheyden, S., Genty, D., Soulier, M., Cheng, H., Blamart, D., Burlet, C., Camus, H., Delaby, S., Deldicque, D., Lawrence Edwards, R., Ferrier, C., Lacrampe-Cuyaubère, F., Lévêque, F., Maksud, F., Mora, P., Muth, X., Régnier, É., Rouzaud, J.-N., Santos, F., 2016. Early Neanderthal constructions deep in Bruniquel cave in southwestern France. Nature 534, 111–115.

Jean-Baptiste, P., Genty, D., Fourré, E., Régnier, E., 2019. Tritium dating of dripwater from Villars Cave (SW-France). Appl. Geochem. 107, 152–158.

Lacanette, D., Vincent, S., Sarthu, A., Malaurent, P., Caltagirone, J.-P., 2009. An Eulerian/Lagrangian method for the numerical simulation of incompressible convection flows interacting with complex obstacles: application to the natural convection in the Lascaux cave. Int. J. Heat Mass Transf. 52, 2528–2542.

Lang, M., Faimon, J., Godissart, J., Ek, C., 2017. Carbon dioxide seasonality in dynamically ventilated caves: the role of advective fluxes. Theor. Appl. Climatol. 129, 1355–1372.

Leplat, J., François, A., Touron, S., Galant, P., Bousta, F., 2019. Aerobiological behavior of Paleolithic decorated caves: a comparative study of five caves in the Gard department (France). Aerobiologia (in press).

Lin, H., 2010. Earth's Critical Zone and hydropedology: concepts, characteristics, and advances. Hydrol. Earth Syst. Sci. 14, 25–45.

Linden, P.F., Lane-Serff, G.F., Smeed, D.A., 1990. Emptying filling boxes: the fluid mechanics of natural ventilation. J. Fluid Mech. 212, 309–335.

Mangin, A., Bourges, F., d'Hulst, D., 1999. Painted caves conservation: a stability problem in a natural system (the example of the prehistoric cave of Gargas, French Pyrenees). C. R. Acad. Sci. Paris 328, 295–301.

Martin-Sanchez, P.M., Nováková, A., Bastian, F., Alabouvette, C., Saiz-Jimenez, C., 2012. Two new species of the genus Ochroconis, O. Lascauxensis and O. anomala isolated from black stains in Lascaux Cave, France. Fungal Biol 116, 574–589.

Martin-Sanchez, P.M., Jurado, V., Porca, E., Bastian, F., Lacanette, D., Alabouvette, C., Saiz-Jimenez, C., 2014. Airborne microorganisms in Lascaux cave (France). Int. J. Speleol. 43, 295–303.

Mattey, D.P., Atkinson, T.C., Barker, J.A., Fisher, R., Latin, J.-P., Durrell, R., Ainsworth, M., 2016. Carbon dioxide, ground air and carbon cycling in Gibraltar karst. Geochim. Cosmochim. Acta 184, 88–113.

Moreau, C., Caffy, I., Comby, C., Delqué-Količ, E., Dumoulin, J.-P., Hain, S., Quiles, A., Setti, V., Souprayen, C., Thellier, B., et al., 2013. Research and development of the Artemis ^{14}C AMS facility: status report. Radiocarbon 55, 648–656.

Perrier, F., 2005. Scaling in convective evaporation and sidewall boundary layer. Eur. Phys. J. B 45, 555–560.
Perrier, F., Le Mouël, J.-L., 2016. Stationary and transient thermal states of barometric pumping in the access pit of an underground quarry. Sci. Tot. Environ. 550, 1044–1056.
Perrier, F., Richon, P., 2010. Spatiotemporal variation of radon and carbon dioxide concentrations in an underground quarry: coupled processes of natural ventilation, barometric pumping and internal mixing. J. Environ. Radioact. 101, 279–296.
Perrier, F., Morat, P., Le Mouël, J.-L., 2001. Pressure induced temperature variations in an underground quarry. Earth Planet. Sci. Lett. 191, 145–156.
Perrier, F., Morat, P., Le Mouël, J.-L., 2002. Dynamics of air avalanches in the access pit of an underground quarry. Phys. Rev. Lett. 89, 134501.
Perrier, F., Morat, P., Yoshino, T., Sano, O., Utada, H., Gensane, O., Le Mouël, J.-L., 2004. Seasonal thermal signatures of heat transfer by water exchange in an underground vault. Geophys. J. Int. 158, 372–384.
Perrier, F., Le Mouël, J.-L., Poirier, J.-P., Shnirman, M.G., 2005. Long-term climate change and surface versus underground temperature measurements in Paris. Int. J. Climatol. 25, 1619–1631.
Perrier, F., Richon, P., Sabroux, J.-C., 2005. Modelling the effect of air exchange on radon-222 and its progeny concentration in a tunnel atmosphere. Sci. Tot. Environ. 350, 136–150.
Perrier, F., Richon, P., Gautam, U., Tiwari, D.R., Shrestha, P., Sapkota, S.N., 2007. Seasonal variations of natural ventilation and radon-222 exhalation flux in a slightly rising dead-end tunnel. J. Environ. Radioact. 97, 220–235.
Perrier, F., Le Mouël, J.-L., Richon, P., 2010. Spatial and temporal dependence of temperature variations induced by atmospheric pressure variations in shallow underground cavities. Pure Appl. Geophys. 167, 253–276.
Peyraube, N., Lastennet, R., Denis, A., Malaurent, P., 2013. Estimation of epikarst air P_{CO2}, using measurements of water $\delta^{13}C_{TDIC}$, cave air P_{CO2}, and $\delta^{13}C_{CO2}$. Geochim. Cosmochim. Acta 118, 1–17.
Peyraube, N., Lastennet, R., Denis, A., Malaurent, P., Houillon, N., Villanueva, J.D., 2018. Determination and quantification of major climatic parameters influencing the CO_2 of Lascaux cave. Theor. App. Climatol. 133, 1291–1301.
Pla, C., 2016. Changes in the CO_2 dynamics in near-surface cavities under a future warming scenario: factors and evidence from the field and experimental findings. Sci. Tot. Environ. 565, 1151–1164.
Quiles, A., Valladas, H., Bocherens, H., Delqué-Količ, E., Kaltnecker, E., van der Plicht, J., Delannoy, J.-J., Feruglio, V., Fritz, C., Monney, J., Philippe, M., Tosello, G., Clottes, J., Geneste, J.-M., 2016. A high-precision chronological model for the decorated Upper Paleolithic cave of Chauvet-Pont d'Arc, Ardèche, France. Proc. Natl. Acad. Sci. U. S. A. 113, 4670–4675.
Quindos, L.S., Bonet, A., Diaz-Caneja, N., Fernandez, P.L., Gutierrez, I., Solana, J.R., Soto, J., Villar, E., 1987. Study of the environmental variables affecting the natural preservation of the Altamira cave paintings located at Santillana Del Mar, Spain. Atm. Environ. 21, 551–560.
Richon, P., Perrier, F., Sabroux, J.-C., Trique, M., Ferry, C., Voisin, V., Pili, E., 2005. Spatial and time variations of radon-222 concentration in the atmosphere of a dead-end horizontal tunnel. J. Environ. Radioact. 78, 179–198.
Richon, P., Perrier, F., Pili, E., Sabroux, J.-C., 2009. Detectability and significance of 12 hr barometric tide in radon-222 signal, dripwater flow rate, air temperature and carbon dioxide concentration in an underground tunnel. Geophys. J. Int. 176, 683–694.
Roberson-Nay, R., Gorlin, E.J., Beadel, J.R., Cash, T., Vrana, S., Teachman, B.A., 2017. Temporal stability of multiple response systems to 7.5% carbon dioxide challenge. Biol. Psychol. 124, 111–118.
Rodriguez-Calcerrada, J., Martin-StPaul, N.K., Lempereur, M., Ourcival, J.-M., del Carmen del Rey, M., Joffre, R., Rambal, S., 2014. Stem CO_2 efflux and its contribution to ecosystem CO_2 efflux decrease with drought in a Mediterranean forest stand. Agric. For. Meteorol. 195–196, 61–72.
Sadier, B., Delannoy, J.-J., Benedetti, L., Bourlès, D.L., Jaillet, S., Geneste, J.-M., Lebatard, A.-E., Arnold, M., 2012. Further constraints on the Chauvet cave artwork elaboration. Proc. Nati. Acad. Sci. 109, 8002–8006.
Saiz-Jimenez, C., Cuezva, S., Jurado, V., Fernandez-Cortes, A., Pora, E., Benavente, D., Cañaveras, J.C., Sanchez-Moral, S., 2011. Paleolithic art in peril: policy and science collide at Altamira cave. Science 334, 42–43.
Sánchez-Cañete, E.P., Serrano-Ortiz, P., Domingo, F., Kowalski, A.S., 2013. Cave ventilation is influenced by variations in the CO_2-dependent virtual temperature. Int. J. Speleol. 42, 1–8.
Sanchez-Moral, S., Soler, V., Cañaveras, J.C., Sanz-Rubio, E., Van Grieken, R., Gysels, K., 1999. Inorganic deterioration affecting the Altamira cave, N Spain: quantitative approach to wall-corrosion (solutional etching) processes induced by visitors. Sci. Tot. Environ. 243/244, 67–84.
Smith, G.K., 1993. Carbon dioxide, caves and you. The Australian Caver 133, 20–23.
Spötl, C., Fairchild, I.J., Tooth, A., 2005. Cave air control on dripwater geochemistry, Obir Caves (Austria): implications for speleothem deposition in dynamically ventilated caves. Geochim. Cosmochim. Acta 69, 2451–2468.
Trias, R., Ménez, B., Le Campion, P., Zivanovic, Y., Lecourt, L., Lecoeuvre, A., Schmitt-Kopplin, P., Uhl, J., Gislason, S.R., Alfredsson, H.E., Mesfin, K.G., Snæbjörndóttir, S., Arradóttir, E.S., Gunnarsson, I., Matter, J.M., Stute, M., Oelkersn, E.H., Gérard, E., 2017. High reactivity of deep biota under atmospheric CO_2 injection into basalt. Nat. Commun. 8, 1063.
Troester, J.W., White, W.B., 1984. Seasonal fluctuations in the carbon dioxide partial pressure in a cave atmosphere. Water Resour. Res. 20, 153–156.
Turner, J.S., 1973. Buoyancy Effects in Fluids. 1980 edition. Cambridge University Press. (408pp).
Valladas, H., Kaltnecker, E., Quiles, A., Tisnerat-Laborde, N., Genty, D., Arnold, M., Delqué-Kolic, E., Moreau, C., Baffier, D., Cleyet-Merle, J.J., Clottes, J., Girard, M., Monney, J., Montes, R., Sainz, C., Sanchidrian, J.L., Simonet, R., 2013. Dating French and Spanish prehistoric decorated caves in their archaeological contexts. Radiocarbon 55, 1422–1431.
Villar, E., Bonet, A., Diaz-Caneja, B., Fernandez, P.L., Gutierrez, I., Quindos, L.S., Solana, J.R., Soto, J., 1984. Ambient temperature variations in the hall of paintings of Altamira cave due to the presence of visitors. Cave Sci 11, 99–104.
Villar, E., Fernandez, P.L., Guttierrez, I., Quindos, L.S., Soto, J., 1986. Influence of visitors on carbon dioxide concentrations in Altamira cave. Cave Sci 13, 21–23.
Vouvé, J., Vouvé, F., Brunet, J., Malaurent, P., 2000. Contribution of in situ colorimetric determination for the characterisation of the prehistorical paintings before the elaboration of a conservation process: the case of the Chauvet cave (Ardèche, France). C. R. Acad. Sci. Paris 331, 627–632.
Wigley, T.M.L., 1967. Non-steady flow through a porous medium and cave breathing. J. Geophys. Res. 72, 3199–3205.
Wood, W.W., 1985. Origin of caves and other solution openings in the unsaturated (vadose) zone of carbonate rocks: a model for CO_2 generation. Geology 13, 822–824.
Wood, W.W., Petraitis, M.J., 1984. Origin and distribution of carbon dioxide in the unsaturated zone of the southern High Plains of Texas. Water Res. Res. 20, 1193–1208.
Zhang, Z., Chen, X., Soulsby, C., 2017. Catchment-scale conceptual modelling of water and solute transport in the dual flow system of the karst critical zone. Hydrol. Proc. 31, 3421–3436.